

DESY 95-143

July 1995

Measurement of Elastic ρ^0 Photoproduction at HERA

The ZEUS Collaboration

Abstract

Elastic ρ^0 photoproduction has been measured using the ZEUS detector at HERA. Untagged photoproduction events from ep interactions were used to measure the reaction $\gamma p \rightarrow \rho^0 p$ ($\rho^0 \rightarrow \pi^+ \pi^-$) at photon-proton centre-of-mass energies between 60 and 80 GeV and $|t| < 0.5 \text{ GeV}^2$, where t is the square of the four-momentum transferred at the proton vertex. The differential cross section $d\sigma/dM_{\pi\pi}$, where $M_{\pi\pi}$ is the invariant mass of the two pions, and the integrated cross section, $\sigma_{\gamma p \rightarrow \rho^0 p}$, are presented; the latter was measured to be 14.7 ± 0.4 (stat.) ± 2.4 (syst.) μb . The differential cross section $d\sigma/dt$ has an approximately exponential shape; a fit of the type $A'_t \exp(-b'_t |t| + c'_t t^2)$ yields a t -slope $b'_t = 9.9 \pm 1.2$ (stat.) ± 1.4 (syst.) μb . The results, when compared to low energy data, show a weak energy dependence of both $\sigma_{\gamma p \rightarrow \rho^0 p}$ and of the t -slope. The ρ^0 is produced predominantly with transverse polarisation, demonstrating that s -channel helicity conservation holds at these energies.

arXiv:hep-ex/9507011v2 20 Jul 1995

The ZEUS Collaboration

M. Derrick, D. Krakauer, S. Magill, D. Mikunas, B. Musgrave, J. Repond, R. Stanek, R.L. Talaga, H. Zhang
Argonne National Laboratory, Argonne, IL, USA^p

R. Ayad¹, G. Bari, M. Basile, L. Bellagamba, D. Boscherini, A. Bruni, G. Bruni, P. Bruni, G. Cara Romeo, G. Castellini², M. Chiarini, L. Cifarelli³, F. Cindolo, A. Contin, M. Corradi, I. Gialas⁴, P. Giusti, G. Iacobucci, G. Laurenti, G. Levi, A. Margotti, T. Massam, R. Nania, C. Nemoz, F. Palmonari, A. Polini, G. Sartorelli, R. Timellini, Y. Zamora Garcia¹, A. Zichichi
University and INFN Bologna, Bologna, Italy^f

A. Bargende⁵, A. Bornheim, J. Crittenden, K. Desch, B. Diekmann⁶, T. Doeker, M. Eckert, L. Feld, A. Frey, M. Geerts, M. Grothe, H. Hartmann, K. Heinloth, E. Hilger, H.-P. Jakob, U.F. Katz, S. Mengel, J. Mollen, E. Paul, M. Pfeiffer, Ch. Rembser, D. Schramm, J. Stamm, R. Wedemeyer
Physikalisches Institut der Universität Bonn, Bonn, Federal Republic of Germany^c

S. Campbell-Robson, A. Cassidy, N. Dyce, B. Foster, S. George, R. Gilmore, G.P. Heath, H.F. Heath, T.J. Llewellyn, C.J.S. Morgado, D.J.P. Norman, J.A. O'Mara, R.J. Tapper, S.S. Wilson, R. Yoshida
H.H. Wills Physics Laboratory, University of Bristol, Bristol, U.K.^o

R.R. Rau
Brookhaven National Laboratory, Upton, L.I., USA^p

M. Arneodo⁷, M. Capua, A. Garfagnini, L. Iannotti, M. Schioppa, G. Susinno
Calabria University, Physics Dept.and INFN, Cosenza, Italy^f

A. Bernstein, A. Caldwell, N. Cartiglia, J.A. Parsons, S. Ritz⁸, F. Sciulli, P.B. Straub, L. Wai, S. Yang, Q. Zhu
Columbia University, Nevis Labs., Irvington on Hudson, N.Y., USA^q

P. Borzemiński, J. Chwastowski, A. Eskreys, K. Piotrkowski, M. Zachara, L. Zawiejski
Inst. of Nuclear Physics, Cracow, Poland^j

L. Adamczyk, B. Bednarek, K. Jeleń, D. Kisielewska, T. Kowalski, E. Rulikowska-Zareńska, L. Suszycki, J. Zając
Faculty of Physics and Nuclear Techniques, Academy of Mining and Metallurgy, Cracow, Poland^j

A. Kotański, M. Przybycień
Jagellonian Univ., Dept. of Physics, Cracow, Poland^k

L.A.T. Bauerdick, U. Behrens, H. Beier⁹, J.K. Bienlein, C. Coldewey, O. Deppe, K. Desler, G. Drews, M. Flasiński¹⁰, D.J. Gilkinson, C. Glasman, P. Göttlicher, J. Große-Knetter, B. Gutjahr¹¹, T. Haas, W. Hain, D. Hasell, H. Heßling, Y. Iga, K. Johnson¹², P. Joos, M. Kasemann, R. Klanner, W. Koch, L. Köpke¹³, U. Kötz, H. Kowalski, J. Labs, A. Ladage, B. Löhner, M. Löwe, D. Lüke, J. Mainusch, O. Mańczak, T. Monteiro¹⁴, J.S.T. Ng, S. Nickel¹⁵, D. Notz, K. Ohrenberg, M. Roco, M. Rohde, J. Roldán, U. Schneekloth, W. Schulz, F. Selonke, E. Stiliaris¹⁶, B. Surrow, T. Voß, D. Westphal, G. Wolf, C. Youngman, W. Zeuner, J.F. Zhou¹⁷
Deutsches Elektronen-Synchrotron DESY, Hamburg, Federal Republic of Germany

H.J. Grabosch, A. Kharchilava, A. Leich, M.C.K. Mattingly, S.M. Mari⁴, A. Meyer, S. Schlenstedt, N. Wulff
DESY-Zeuthen, Inst. für Hochenergiephysik, Zeuthen, Federal Republic of Germany

G. Barbagli, P. Pelfer
University and INFN, Florence, Italy^f

G. Anzivino, G. Maccarrone, S. De Pasquale, L. Votano
INFN, Laboratori Nazionali di Frascati, Frascati, Italy^f

A. Bamberger, S. Eisenhardt, A. Freidhof, S. Söldner-Rembold¹⁸, J. Schroeder¹⁹, T. Trefzger
Fakultät für Physik der Universität Freiburg i.Br., Freiburg i.Br., Federal Republic of Germany^c

N.H. Brook, P.J. Bussey, A.T. Doyle²⁰, D.H. Saxon, M.L. Utley, A.S. Wilson
Dept. of Physics and Astronomy, University of Glasgow, Glasgow, U.K. ^o

A. Dannemann, U. Holm, D. Horstmann, T. Neumann, R. Sinkus, K. Wick
Hamburg University, I. Institute of Exp. Physics, Hamburg, Federal Republic of Germany ^c

E. Badura²¹, B.D. Burow²², L. Hagge, E. Lohrmann, J. Milewski, M. Nakahata²³, N. Pavel, G. Poelz, W. Schott, F. Zetsche
Hamburg University, II. Institute of Exp. Physics, Hamburg, Federal Republic of Germany ^c

T.C. Bacon, N. Bruemmer, I. Butterworth, E. Gallo, V.L. Harris, B.Y.H. Hung, K.R. Long, D.B. Miller, P.P.O. Morawitz, A. Priniyas, J.K. Sedgbeer, A.F. Whitfield
Imperial College London, High Energy Nuclear Physics Group, London, U.K. ^o

U. Mallik, E. McCliment, M.Z. Wang, S.M. Wang, J.T. Wu
University of Iowa, Physics and Astronomy Dept., Iowa City, USA ^p

P. Cloth, D. Filges
Forschungszentrum Jülich, Institut für Kernphysik, Jülich, Federal Republic of Germany

S.H. An, S.M. Hong, S.W. Nam, S.K. Park, M.H. Suh, S.H. Yon
Korea University, Seoul, Korea ^h

R. Imlay, S. Kartik, H.-J. Kim, R.R. McNeil, W. Metcalf, V.K. Nadendla
Louisiana State University, Dept. of Physics and Astronomy, Baton Rouge, LA, USA ^p

F. Barreiro²⁴, G. Cases, J.P. Fernandez, R. Graciani, J.M. Hernández, L. Hervás²⁴, L. Labarga²⁴, M. Martinez, J. del Peso, J. Puga, J. Terron, J.F. de Trocóniz
Univer. Autónoma Madrid, Depto de Física Teórica, Madrid, Spain ⁿ

G.R. Smith
University of Manitoba, Dept. of Physics, Winnipeg, Manitoba, Canada ^a

F. Corriveau, D.S. Hanna, J. Hartmann, L.W. Hung, J.N. Lim, C.G. Matthews, P.M. Patel, L.E. Sinclair, D.G. Stairs, M. St-Laurent, R. Ullmann, G. Zacek
McGill University, Dept. of Physics, Montréal, Québec, Canada ^{a, b}

V. Bashkirov, B.A. Dolgoshein, A. Stifutkin
Moscow Engineering Physics Institute, Moscow, Russia ^l

G.L. Bashindzhagyan, P.F. Ermolov, L.K. Gladilin, Yu.A. Golubkov, V.D. Kobrin, I.A. Korzhavina, V.A. Kuzmin, O.Yu. Lukina, A.S. Proskuryakov, A.A. Savin, L.M. Shcheglova, A.N. Solomin, N.P. Zotov
Moscow State University, Institute of Nuclear Physics, Moscow, Russia ^m

M. Botje, F. Chlebana, A. Dake, J. Engelen, M. de Kamps, P. Kooijman, A. Kruse, H. Tiecke, W. Verkerke, M. Vreeswijk, L. Wiggers, E. de Wolf, R. van Woudenberg
NIKHEF and University of Amsterdam, Netherlands ⁱ

D. Acosta, B. Bylsma, L.S. Durkin, J. Gilmore, K. Honscheid, C. Li, T.Y. Ling, K.W. McLean²⁵, W.N. Murray, P. Nylander, I.H. Park, T.A. Romanowski²⁶, R. Seidlein²⁷
Ohio State University, Physics Department, Columbus, Ohio, USA ^p

D.S. Bailey, A. Byrne²⁸, R.J. Cashmore, A.M. Cooper-Sarkar, R.C.E. Devenish, N. Harnew, M. Lancaster, L. Lindemann⁴, J.D. McFall, C. Nath, V.A. Noyes, A. Quadt, J.R. Tickner, H. Uijterwaal, R. Walczak, D.S. Waters, F.F. Wilson, T. Yip
Department of Physics, University of Oxford, Oxford, U.K. ^o

G. Abbiendi, A. Bertolin, R. Brugnera, R. Carlin, F. Dal Corso, M. De Giorgi, U. Dosselli, S. Limentani, M. Morandin, M. Posocco, L. Stanco, R. Stroili, C. Voci
Dipartimento di Fisica dell' Università and INFN, Padova, Italy ^f

J. Bulmahn, J.M. Butterworth, R.G. Feild, B.Y. Oh, J.J. Whitmore²⁹
Pennsylvania State University, Dept. of Physics, University Park, PA, USA^q

G. D'Agostini, G. Marini, A. Nigro, E. Tassi
Dipartimento di Fisica, Univ. 'La Sapienza' and INFN, Rome, Italy^f

J.C. Hart, N.A. McCubbin, K. Prytz, T.P. Shah, T.L. Short
Rutherford Appleton Laboratory, Chilton, Didcot, Oxon, U.K.^o

E. Barberis, T. Dubbs, C. Heusch, M. Van Hook, W. Lockman, J.T. Rahn, H.F.-W. Sadrozinski, A. Seiden, D.C. Williams
University of California, Santa Cruz, CA, USA^p

J. Biltzinger, R.J. Seifert, O. Schwarzer, A.H. Walenta, G. Zech
Fachbereich Physik der Universität-Gesamthochschule Siegen, Federal Republic of Germany^c

H. Abramowicz, G. Briskin, S. Dagan³⁰, A. Levy³¹
School of Physics, Tel-Aviv University, Tel Aviv, Israel^e

J.I. Fleck, T. Hasegawa, M. Hazumi, T. Ishii, M. Kuze, S. Mine, Y. Nagasawa, M. Nakao, I. Suzuki, K. Tokushuku, S. Yamada, Y. Yamazaki
Institute for Nuclear Study, University of Tokyo, Tokyo, Japan^g

M. Chiba, R. Hamatsu, T. Hirose, K. Homma, S. Kitamura, Y. Nakamitsu, K. Yamauchi
Tokyo Metropolitan University, Dept. of Physics, Tokyo, Japan^g

R. Cirio, M. Costa, M.I. Ferrero, L. Lamberti, S. Maselli, C. Peroni, R. Sacchi, A. Solano, A. Staiano
Universita di Torino, Dipartimento di Fisica Sperimentale and INFN, Torino, Italy^f

M. Dardo
II Faculty of Sciences, Torino University and INFN - Alessandria, Italy^f

D.C. Bailey, D. Bandyopadhyay, F. Benard, M. Brkic, D.M. Gingrich³², G.F. Hartner, K.K. Joo, G.M. Levman, J.F. Martin, R.S. Orr, S. Polenz, C.R. Sampson, R.J. Teuscher
University of Toronto, Dept. of Physics, Toronto, Ont., Canada^a

C.D. Catterall, T.W. Jones, P.B. Kaziewicz, J.B. Lane, R.L. Saunders, J. Shulman
University College London, Physics and Astronomy Dept., London, U.K.^o

K. Blankenship, B. Lu, L.W. Mo
Virginia Polytechnic Inst. and State University, Physics Dept., Blacksburg, VA, USA^q

W. Bogusz, K. Charchuła, J. Ciborowski, J. Gajewski, G. Grzelak, M. Kasprzak, M. Krzyżanowski, K. Muchorowski, R.J. Nowak, J.M. Pawlak, T. Tymieniecka, A.K. Wróblewski, J.A. Zakrzewski, A.F. Żarnecki
Warsaw University, Institute of Experimental Physics, Warsaw, Poland^j

M. Adamus
Institute for Nuclear Studies, Warsaw, Poland^j

Y. Eisenberg³⁰, U. Karshon³⁰, D. Revel³⁰, D. Zer-Zion
Weizmann Institute, Nuclear Physics Dept., Rehovot, Israel^d

I. Ali, W.F. Badgett, B. Behrens, S. Dasu, C. Fordham, C. Foudas, A. Goussiou, R.J. Loveless, D.D. Reeder, S. Silverstein, W.H. Smith, A. Vaiciulis, M. Wodarczyk
University of Wisconsin, Dept. of Physics, Madison, WI, USA^p

T. Tsurugai
Meiji Gakuin University, Faculty of General Education, Yokohama, Japan

S. Bhadra, M.L. Cardy, C.-P. Fagerstroem, W.R. Frisken, K.M. Furutani, M. Khakzad, W.B. Schmidke
York University, Dept. of Physics, North York, Ont., Canada^a

- ¹ supported by Worldlab, Lausanne, Switzerland
- ² also at IROE Florence, Italy
- ³ now at Univ. of Salerno and INFN Napoli, Italy
- ⁴ supported by EU HCM contract ERB-CHRX-CT93-0376
- ⁵ now at Möbelhaus Kramm, Essen
- ⁶ now a self-employed consultant
- ⁷ now also at University of Torino
- ⁸ Alfred P. Sloan Foundation Fellow
- ⁹ presently at Columbia Univ., supported by DAAD/HSPH-AUFE
- ¹⁰ now at Inst. of Computer Science, Jagellonian Univ., Cracow
- ¹¹ now at Comma-Soft, Bonn
- ¹² visitor from Florida State University
- ¹³ now at Univ. of Mainz
- ¹⁴ supported by DAAD and European Community Program PRAXIS XXI
- ¹⁵ now at Dr. Seidel Informationssysteme, Frankfurt/M.
- ¹⁶ now at Inst. of Accelerating Systems & Applications (IASA), Athens
- ¹⁷ now at Mercer Management Consulting, Munich
- ¹⁸ now with OPAL Collaboration, Faculty of Physics at Univ. of Freiburg
- ¹⁹ now at SAS-Institut GmbH, Heidelberg
- ²⁰ also supported by DESY
- ²¹ now at GSI Darmstadt
- ²² also supported by NSERC
- ²³ now at Institute for Cosmic Ray Research, University of Tokyo
- ²⁴ partially supported by CAM
- ²⁵ now at Carleton University, Ottawa, Canada
- ²⁶ now at Department of Energy, Washington
- ²⁷ now at HEP Div., Argonne National Lab., Argonne, IL, USA
- ²⁸ now at Oxford Magnet Technology, Eynsham, Oxon
- ²⁹ on leave and partially supported by DESY 1993-95
- ³⁰ supported by a MINERVA Fellowship
- ³¹ partially supported by DESY
- ³² now at Centre for Subatomic Research, Univ. of Alberta, Canada and TRIUMF, Vancouver, Canada

- a* supported by the Natural Sciences and Engineering Research Council of Canada (NSERC)
- b* supported by the FCAR of Québec, Canada
- c* supported by the German Federal Ministry for Research and Technology (BMFT)
- d* supported by the MINERVA Gesellschaft für Forschung GmbH, and by the Israel Academy of Science
- e* supported by the German Israeli Foundation, and by the Israel Academy of Science
- f* supported by the Italian National Institute for Nuclear Physics (INFN)
- g* supported by the Japanese Ministry of Education, Science and Culture (the Monbusho) and its grants for Scientific Research
- h* supported by the Korean Ministry of Education and Korea Science and Engineering Foundation
- i* supported by the Netherlands Foundation for Research on Matter (FOM)
- j* supported by the Polish State Committee for Scientific Research (grant No. SPB/P3/202/93) and the Foundation for Polish- German Collaboration (proj. No. 506/92)
- k* supported by the Polish State Committee for Scientific Research (grant No. PB 861/2/91 and No. 2 2372 9102, grant No. PB 2 2376 9102 and No. PB 2 0092 9101)
- l* partially supported by the German Federal Ministry for Research and Technology (BMFT)
- m* supported by the German Federal Ministry for Research and Technology (BMFT), the Volkswagen Foundation, and the Deutsche Forschungsgemeinschaft
- n* supported by the Spanish Ministry of Education and Science through funds provided by CICYT
- o* supported by the Particle Physics and Astronomy Research Council
- p* supported by the US Department of Energy
- q* supported by the US National Science Foundation

1 Introduction

“Elastic” or “exclusive” production of ρ^0 mesons by photons, $\gamma p \rightarrow \rho^0 p$, has been extensively studied in fixed target experiments up to photon-proton centre-of-mass energies $W \simeq 20$ GeV, using both real and virtual photons [1]-[31]. Recently, the cross section for this reaction has also been obtained in an indirect measurement at the HERA ep collider, using quasi-real photons with space-like virtuality Q^2 between $4 \cdot 10^{-8}$ and $2 \cdot 10^{-2}$ GeV², at an average centre-of-mass energy $\langle W \rangle$ of 180 GeV [32].

At W values up to about 20 GeV, elastic photoproduction of ρ^0 mesons has the characteristic features of soft diffractive processes: the dependence of the production cross section on W is weak, the dependence on t , the square of the four-momentum transferred at the proton vertex, is approximately exponential, and the vector meson is observed to retain the helicity of the photon (s -channel helicity conservation, SCHC). Such energy and t dependences are also characteristic of hadronic diffractive processes. The similarity between ρ^0 photoproduction and hadronic processes can be understood in the framework of the Vector Dominance Model (VDM) [33], in which the photon is assumed to fluctuate into a vector meson before interacting with the target nucleon; the reaction $\gamma p \rightarrow \rho^0 p$ is thus related to the elastic process $\rho^0 p \rightarrow \rho^0 p$.

At sufficiently high energies, diffractive interactions are usually described in terms of the exchange of a pomeron, an object with the quantum numbers of the vacuum. Regge theory provides a framework in which many of the features of hadronic reactions can be described [34]. In particular, the energy dependence of diffractive processes is related to the intercept of the pomeron trajectory. Several models offer a description of diffractive vector meson production [35]-[41]; some of them are in the framework of perturbative QCD. The study of vector meson photoproduction at the energies available at HERA may thus help to clarify the nature of the pomeron.

This paper reports a measurement of the elastic ρ^0 photoproduction cross section at $\langle W \rangle$ of 70 GeV, based on about 6,000 $ep \rightarrow ep\pi^+\pi^-$ events collected by the ZEUS experiment in 1993. In this measurement the final state electron and proton are not detected and the relevant kinematic quantities are determined from the measured three-momenta of the ρ^0 decay products, assuming that they are pions.

The paper is organised as follows. After defining the variables relevant to ρ^0 production, we describe the experimental conditions and the event selection criteria, and then discuss the acceptance corrections and the background. From the analysis of the differential cross section $d\sigma/dM_{\pi\pi}$, where $M_{\pi\pi}$ is the invariant mass of the $\pi^+\pi^-$ system, we obtain the integrated cross section $\sigma_{\gamma p \rightarrow \rho^0 p}$. We then discuss the differential cross section $d\sigma/dt$ and the angular distributions of the decay pions. Finally, from the value of $d\sigma/dt$ at $t = 0$, the total $\rho^0 p$ cross section is derived using the optical theorem and assuming VDM.

2 Elastic ρ^0 photoproduction at HERA

Elastic ρ^0 photoproduction was investigated by means of the reaction (see Fig. 1)

$$e(k) + p(P) \rightarrow e(k') + \rho^0(V) + p(P'),$$

where the symbols in parenthesis indicate the four-momenta of the particles involved.

For unpolarised electrons and protons, two independent variables describe inclusive ep scattering, since the ep centre-of-mass energy $\sqrt{s} = 2\sqrt{E_e E_p} = 296$ GeV is fixed by the energies of the electron (E_e) and of the proton (E_p) beams. The variables can be any two of the following four:

- $-Q^2 = q^2 = (k - k')^2$, the four-momentum squared carried by the virtual photon;
- $x = Q^2/(2P \cdot q)$, the Bjorken variable;
- $y = (q \cdot P)/(k \cdot P)$, the fraction of the electron energy transferred by the photon to the hadronic final state, measured in the proton rest frame;
- W , the centre-of-mass energy of the γ^*p system, where

$$W^2 = (q + P)^2 = -Q^2 + 2y(k \cdot P) + M_p^2,$$

M_p being the proton mass.

The hadronic final state, containing the scattered proton and the pions from the decay $\rho^0 \rightarrow \pi^+\pi^-$, is described by additional variables, including the invariant mass $M_{\pi\pi}$ of the two decay pions, the square of the four-momentum transferred at the proton vertex, t , and the polar and azimuthal angles, defined in section 7.4, of the decay pions in the $\pi\pi$ centre-of-mass frame.

For the data presented here, only the three-momenta of the final state pions were measured. Events in which the scattered electron was detected in the ZEUS calorimeter were rejected, thereby restricting Q^2 to be below $Q_{\max}^2 \approx 4$ GeV². The median Q^2 is approximately 10^{-4} GeV². To explain how the relevant kinematic quantities are obtained from the four-momenta of the two pions, we first consider the case $Q^2 = Q_{\min}^2 = M_e^2 \frac{y^2}{1-y}$ (M_e is the electron mass) and then discuss the effect of larger Q^2 . For $Q^2 = Q_{\min}^2$ ($\approx 10^{-9}$ GeV² for the kinematic range covered by the present data), the virtual photon is emitted with zero transverse momentum and with longitudinal momentum $p_{Z\gamma} \simeq -E_\gamma$ in the direction opposite to that of the proton beam¹. Energy and momentum conservation relate the photon energy E_γ to the two-pion system energy $E_{\pi\pi}$ and longitudinal momentum $p_{Z\pi\pi}$ by $2E_\gamma \simeq (E_{\pi\pi} - p_{Z\pi\pi})$. The photon-proton centre-of-mass energy can then be expressed as:

$$W^2 \simeq 4E_\gamma E_p \simeq 2(E_{\pi\pi} - p_{Z\pi\pi})E_p.$$

The ρ^0 transverse momentum squared in the laboratory frame, p_T^2 , approximates to $-t$:

$$\begin{aligned} t &= (q - V)^2 = -Q^2 - 2q \cdot V + M_{\pi\pi}^2 \\ &\simeq -2E_\gamma(E_{\pi\pi} + p_{Z\pi\pi}) + M_{\pi\pi}^2 \\ &\simeq -(E_{\pi\pi}^2 - p_{Z\pi\pi}^2) + M_{\pi\pi}^2 \\ &= -p_T^2, \end{aligned}$$

¹Throughout this paper we use the standard ZEUS right-handed coordinate system, in which $X = Y = Z = 0$ is the nominal interaction point, the positive Z -axis points in the direction of flight of the protons (referred to as the forward direction) and the X -axis is horizontal, pointing towards the centre of HERA.

where, in addition to $2E_\gamma \simeq (E_{\pi\pi} - p_{Z\pi\pi})$, we have used the approximation $Q^2 = 0$. Non-zero values of Q^2 cause p_T^2 to differ from $-t$ by $\lesssim Q^2$; the effect on the measured distributions is discussed in section 5. For this measurement, the minimum kinematically allowed value of $|t|$ is negligible, $|t_{\min}| \simeq 10^{-8}$ GeV² at $W = 70$ GeV.

Fig. 2 shows the scatter plot of the reconstructed versus the true values of W and t for the sample of Monte Carlo events used to evaluate the acceptance (cf. section 5). The difference of the reconstructed and the true value of W has a mean value of zero and an r.m.s. spread of 1.4 GeV. The analogous difference for t has also a mean value of approximately zero and an r.m.s. spread of 0.06 GeV². The events far from the diagonal have $Q^2 \gg Q_{\min}^2$. Throughout the analysis, the variable W was calculated using the above approximation. For t , the Q^2 dependence of the relation between t and p_T^2 was taken into account in the acceptance correction, as discussed in section 5.

In the one photon exchange approximation, the ep and the γ^*p cross sections for elastic ρ^0 production are related by

$$\frac{d^2\sigma_{ep \rightarrow ep\rho^0}}{dydQ^2} = \frac{\alpha}{2\pi Q^2} \left[\left(\frac{1 + (1-y)^2}{y} - \frac{2(1-y)}{y} \cdot \frac{Q_{\min}^2}{Q^2} \right) \cdot \sigma_T^{\gamma^*p \rightarrow \rho^0 p}(W, Q^2) + \frac{2(1-y)}{y} \cdot \sigma_L^{\gamma^*p \rightarrow \rho^0 p}(W, Q^2) \right], \quad (1)$$

where α is the fine structure constant and $\sigma_T^{\gamma^*p \rightarrow \rho^0 p}(W, Q^2)$ and $\sigma_L^{\gamma^*p \rightarrow \rho^0 p}(W, Q^2)$ are the respective cross sections for transversely and longitudinally polarised virtual photons. Following VDM, these are related by

$$\sigma_L^{\gamma^*p \rightarrow \rho^0 p}(W, Q^2) \simeq \sigma_T^{\gamma^*p \rightarrow \rho^0 p}(W, Q^2) \cdot \frac{Q^2}{M_\rho^2}, \quad (2)$$

with

$$\sigma_T^{\gamma^*p \rightarrow \rho^0 p}(W, Q^2) = \sigma_{\gamma p \rightarrow \rho^0 p}(W) \left/ \left(1 + \frac{Q^2}{M_\rho^2} \right)^2 \right., \quad (3)$$

where $\sigma_{\gamma p \rightarrow \rho^0 p}(W)$ is the cross section for elastic photoproduction ($Q^2 = 0$) of ρ^0 mesons, and M_ρ is the ρ^0 meson mass. Substituting the latter two expressions into equation (1) yields:

$$\frac{d^2\sigma_{ep \rightarrow ep\rho^0}}{dydQ^2} = \Phi(y, Q^2) \cdot \sigma_{\gamma p \rightarrow \rho^0 p}(W(y)), \quad (4)$$

where the function

$$\Phi(y, Q^2) = \frac{\alpha}{2\pi Q^2} \left\{ \left[\frac{1 + (1-y)^2}{y} - \frac{2(1-y)}{y} \left(\frac{Q_{\min}^2}{Q^2} - \frac{Q^2}{M_\rho^2} \right) \right] \frac{1}{\left(1 + \frac{Q^2}{M_\rho^2} \right)^2} \right\} \quad (5)$$

is the effective photon flux.

The cross section $\sigma_{\gamma p \rightarrow \rho^0 p}(\langle W \rangle)$ for elastic ρ^0 photoproduction is thus obtained as the ratio of the corresponding acceptance corrected electron-proton cross-section, integrated over the y and Q^2 ranges covered by the measurement, and the effective photon flux $\Phi(y, Q^2)$ integrated over the same y and Q^2 ranges. This procedure determines the cross section, assuming VDM, for elastic production of ρ^0 mesons at $Q^2 = 0$ averaged over the W range of the measurement.

3 Experimental conditions

3.1 HERA

During 1993, HERA operated at a proton energy of 820 GeV and an electron energy of 26.7 GeV; 84 colliding electron-proton bunches were stored, with an additional 6 unpaired proton and 10 unpaired electron bunches. These additional pilot bunches were used for background studies. The time between bunch crossings was 96 ns. Typical bunch currents were 10 mA for both the electron and the proton beam, providing luminosities of approximately $6 \cdot 10^{29} \text{ cm}^{-2} \text{ s}^{-1}$.

3.2 The ZEUS detector

The components of the ZEUS detector are described in detail in ref. [42]. A short description of those most relevant to the present analysis follows.

Charged particles are tracked by the vertex detector (VXD) and the central tracking detector (CTD) which operate in a magnetic field of 1.43 T provided by a thin superconducting solenoid. The VXD [43] is a cylindrical drift chamber that surrounds the beam pipe and consists of 120 radial cells, each with 12 sense wires. The VXD resolution in the plane transverse to the beam direction, for the data presented here, is $50 \mu\text{m}$ in the central region of a cell and $150 \mu\text{m}$ near the cell edges. The CTD [44] consists of 72 cylindrical drift chamber layers, organised in 9 superlayers covering the polar angle region $15^\circ < \theta < 164^\circ$. In 1993, the spatial resolution in the plane perpendicular to the beam was $\simeq 260 \mu\text{m}$. For the data presented in this paper, the combined CTD and VXD information provides resolutions for the primary ep interaction vertex of 1.1 cm in Z and 0.2 cm in the XY plane. The momentum resolution, for tracks traversing all superlayers, is $\sigma(p_t)/p_t \approx \sqrt{(0.005)^2 p_t^2 + (0.016)^2}$, where p_t is in GeV.

The high resolution uranium-scintillator calorimeter (CAL) [45] consists of a forward (FCAL), a barrel (BCAL) and a rear (RCAL) part, respectively covering the polar regions 2.2° to 36.7° , 36.7° to 129.1° , and 129.1° to 176.6° . The calorimeter parts are subdivided transversely into towers and longitudinally into electromagnetic (EMC) and hadronic (HAC) sections. A section of a tower is called a cell; each cell is viewed by two photomultiplier tubes. Holes of $20 \times 20 \text{ cm}^2$ in the centre of FCAL and RCAL accommodate the HERA beam pipe. From test beam data, the energy resolution was found to be $\sigma_E/E = 0.18/\sqrt{E(\text{GeV})}$ for electrons and $\sigma_E/E = 0.35/\sqrt{E(\text{GeV})}$ for hadrons. The performance, energy and time calibration of the calorimeter are continuously monitored using pedestal triggers, charge and light injection as well as the uranium radioactivity. The additional features relevant to the present analysis are the sub-nanosecond time resolution and the low noise of approximately 15 MeV for the electromagnetic and 25 MeV for the hadronic cells.

The veto wall is used to tag events in which a proton has scattered off a residual gas molecule in the beam pipe (“proton-gas” events) upstream of the ZEUS detector. It consists of two layers of scintillators, with overall dimensions of $500 \text{ cm} \times 600 \text{ cm}$, on both sides of an 87 cm thick iron wall centred at $Z = -7.3 \text{ m}$.

The C5 beam monitor, a small lead-scintillator counter assembly located at $Z = -3.2 \text{ m}$, records the arrival times of halo particles associated with the proton and electron bunches

within 10 cm of the beam axis. It is used to verify the relative timing of the beams and to reject events due to proton-gas interactions.

The luminosity detector (LUMI) [46] measures the luminosity by means of the Bethe-Heitler reaction $ep \rightarrow ep\gamma$; a detailed description of the method used is given in [32]. The bremsstrahlung events are identified by measuring the radiated photon in a lead-scintillator calorimeter placed in the HERA tunnel downstream of the interaction point in the direction of the outgoing electron.

3.3 Untagged ρ^0 photoproduction trigger

ZEUS uses a three level trigger system [42]. The data presented here come from the “untagged photoproduction trigger”, designed to select vector meson photoproduction events [47]. The term “untagged” refers to the fact that the scattered electron escapes undetected through the beam pipe hole in the RCAL and is not detected in the LUMI detector.

The trigger conditions can be summarised as follows:

- First-level-trigger (FLT):
 - At least 464 MeV deposited in the electromagnetic section of RCAL.
 - At least one track candidate in the CTD.
 - Less than 3750 MeV deposited in the calorimeter towers surrounding the beam pipe in the forward direction. This requirement suppressed proton beam-gas events and a significant fraction of the photoproduction cross section.

The trigger was vetoed if hits were present in the C5 or in the veto wall counters, with timing consistent with that of a p -gas collision occurred upstream of the interaction point.

The resulting FLT rate was ≈ 10 Hz at a luminosity of $6 \cdot 10^{29} \text{ cm}^{-2} \text{ s}^{-1}$.

- Second-level-trigger (SLT):
 - Events with calorimeter timing indicating that the interaction had occurred upstream of the interaction point were rejected.
- Third-level-trigger (TLT):
 - Cosmic ray events were discarded on the basis of calorimeter timing.
 - A tighter calorimeter timing rejection was applied.
 - A cut on the Z value of the reconstructed event vertex of ± 85 cm was imposed.

The rate of events passing the untagged photoproduction trigger at the third level was about 1.2 Hz. For some fraction of the data-taking period a factor of 3 prescale was applied.

The requirements that a signal be detected in RCAL and a track be seen in the CTD effectively selected events with photon energies between 0.5 and 4 GeV, corresponding to $40 < W < 120$ GeV.

4 Event selection

During 1993, approximately $7 \cdot 10^6$ events were recorded, corresponding to a total integrated luminosity of about 550 nb^{-1} . The data presented in this paper correspond to an effective luminosity, accounting for the effects of the prescaling of the trigger mentioned in the previous section, of $(240 \pm 8) \text{ nb}^{-1}$.

The following offline requirements were imposed in order to obtain the final ρ^0 photoproduction sample:

- exactly two tracks from particles of opposite charge and both associated with a reconstructed vertex;
- transverse momentum greater than 200 MeV and hits in at least the 3 innermost CTD superlayers for each of the two tracks, thus restricting the data to a region of well understood track reconstruction efficiency; this restriction approximately translates into one on the track pseudorapidity ($\eta = -\ln \tan \theta/2$) of $|\eta| \lesssim 1.8$;
- vertex position within ± 40 cm of the nominal interaction point and within a radial distance of 1.5 cm from the beam axis (the interaction region was centred at $Z = -6$ cm and had an r.m.s. width of ± 11 cm);
- total energy in the forward calorimeter $E_{FCAL} \leq 1$ GeV, thereby limiting the contamination from the reaction $ep \rightarrow e\rho^0 X$, where X is a hadronic state of mass M_X into which the proton had dissociated;
- no energy deposits larger than 200 MeV in any calorimeter cell outside a circular region around the track impact point with a radius of 30 cm in the EMC and 50 cm in the HAC, thus rejecting events with neutral particles or with charged particles outside the region of sensitivity of the tracking system.

A total of 13570 events satisfied the above criteria.

The pion mass was assigned to each track and the analysis was restricted to events reconstructed in the kinematic region defined by:

$$\begin{aligned}
 60 < W < 80 \text{ GeV}, \\
 0.55 < M_{\pi\pi} < 1.0 \text{ GeV}, \\
 p_T^2 < 0.5 \text{ GeV}^2.
 \end{aligned}
 \tag{6}$$

In the chosen energy range the acceptance is well understood. The restricted mass range reduces the contamination from reactions involving other vector mesons, in particular from elastic ϕ and ω production, as well as from photon conversions. The restricted p_T range reduces the contamination from events with diffractive dissociation of the proton ($ep \rightarrow e\rho^0 X$). The final sample contains 6381 events.

The invariant mass spectrum is shown in Fig. 3 before and after the offline selection. The data are dominated by the ρ^0 signal. The corresponding mass spectra of like-sign two track events are also shown as the shaded areas. The small peak just above the $\pi\pi$ threshold in Figs. 3b and c is due to $\phi \rightarrow K^+K^-$ events, where the pion mass has been erroneously assigned to the tracks.

5 Monte Carlo generators and acceptance calculation

The reaction $ep \rightarrow e\rho^0 p$ was modelled using two different Monte Carlo generators.

The first generator, DIPSI [48], describes ρ^0 photoproduction in terms of pomeron exchange. Based on the model of Ryskin [37], it assumes that the exchanged photon fluctuates into a $q\bar{q}$ pair which then interacts with the pomeron emitted by the incident proton. The pomeron is described in terms of a gluon ladder. The cross section is proportional to $[\alpha_s(\bar{q}^2)]^2 \cdot [\bar{x}g(\bar{x}, \bar{q}^2)]^2$, where $\alpha_s(\bar{q}^2)$ is the strong coupling constant, $\bar{x}g(\bar{x}, \bar{q}^2)$ is the gluon momentum density in the proton, \bar{x} is the fraction of the proton's momentum carried by the gluon ladder and $2\bar{q}^2$, in the leading logarithm approximation, is the upper limit for the virtuality of the two t -channel gluons of the gluon ladder. Once α_s and the gluon momentum density are fixed, the W and t dependences are determined. The process under study is sensitive to values of $\bar{x} \approx M_\rho^2/W^2 \approx 10^{-4}$ and $\bar{q}^2 \approx 0.25 M_\rho^2 \approx 0.15 \text{ GeV}^2$. The latter is below the expected region of validity of the calculation; a parametrisation for the product $[\alpha_s(\bar{q}^2)]^2 \cdot [\bar{x}g(\bar{x}, \bar{q}^2)]^2$ was however found for which the model describes all measured distributions well [49]. For this choice of the parameters the cross section has a very weak dependence on W . The two-pion invariant mass $M_{\pi\pi}$ was generated so as to reproduce, after reconstruction, the measured distribution.

The second generator, LEVEC, was developed within the HERWIG framework [50]. It assumes expression (3) for the Q^2 dependence of the cross section; the contribution of longitudinal photons is neglected. The generated events were weighted such that all other distributions (i.e. those over W , $M_{\pi\pi}$, p_T^2 and the angular distributions of the decay pions), after detector simulation and event reconstruction, have the same shape as those of the data.

For both programs, the angular distribution of the decay pions was assumed to be that expected on the basis of SCHC [51].

The acceptance for elastic ρ^0 production was calculated using both the DIPSI and the LEVEC generators. Fig. 4a, b and c respectively show the acceptance as a function of $M_{\pi\pi}$, W and p_T^2 . The acceptance includes the effects of the geometric acceptance of the apparatus, of the detector efficiency and resolution, and of the trigger and reconstruction efficiencies. The trigger efficiency is $\approx 43\%$. The average acceptance is about 7%. The acceptance increases with increasing $\pi\pi$ mass, has a broad maximum for $W \lesssim 70 \text{ GeV}$ and is almost independent of the ρ^0 transverse momentum squared. In order to convert the measured dN/dp_T^2 distribution to the differential cross section $d\sigma/dt$, the p_T^2 acceptance (Fig. 4c) was multiplied by a correction factor F , which is, bin by bin, the ratio of the p_T^2 and t distributions at the generator level. Fig. 4d shows F as a function of p_T^2 .

To produce the acceptance corrected cross sections, the generator DIPSI was used. The difference between the results for the acceptance obtained with the two generators was taken as an estimate of the systematic error due to the model dependence of the acceptance calculation.

From the comparison of the distributions of the reconstructed and generated events, the resolutions in $M_{\pi\pi}$ and p_T^2 were found to be $\sigma_{M_{\pi\pi}} \simeq 20 \text{ MeV}$ – consistent with the mass widths found for neutral strange particles reconstructed using the CTD information [52] – and $\sigma_{p_T^2} \simeq 0.01 \text{ GeV}^2$.

The DIPSI and LEVEC simulations were also used to produce samples of elastic ω and ϕ photoproduction events for the study of the contamination from such processes.

The reaction $ep \rightarrow e\rho^0 X$, where X is the hadronic state resulting from the diffractive dissociation of the proton (see section 6), was simulated using PYTHIA [53]. A cross section of the form $d^2\sigma/dtdM_X^2 \propto e^{bt}/M_X^\beta$, with $b = 4.5 \text{ GeV}^{-2}$, was assumed; the maximum value of M_X was fixed by the condition $M_X^2/W^2 \leq 0.1$ [54]. The exponent β was varied between 2 and 3, consistent with the result $\beta = 2.20 \pm 0.03$ recently obtained at Fermilab [55] for the diffractive dissociation of the proton in $\bar{p}p$ collisions. A second generator (RHODI) was also used, based on the model calculation of ref. [56]. In both generators the ρ^0 decay angular distributions were assumed to be the same as those of the elastic events.

6 Backgrounds

After applying the selection criteria described in section 4, the data still contain contributions from various background processes to the reaction $ep \rightarrow e\pi^+\pi^-p$:

- inelastic ρ^0 production, $ep \rightarrow e\rho^0 X$, in which the proton diffractively dissociates into a hadronic state X not detected in the calorimeter;
- elastic production of ω and ϕ mesons;
- beam-gas interactions.

In order to estimate the contamination from the inelastic channel $ep \rightarrow e\rho^0 X$, the energy distribution in the forward calorimeter (E_{FCAL}) was studied. Fig. 5 shows the distributions for both elastic and inelastic events as obtained from Monte Carlo simulations based on the generators described above, along with the distribution for the data. To obtain these plots, the cut $E_{FCAL} < 1 \text{ GeV}$ was not applied. The plot for elastic Monte Carlo events (Fig. 5a) shows the FCAL energy spectrum resulting from noise (mainly the uranium radioactivity). Nearly all events have $E_{FCAL} < 1 \text{ GeV}$. For the inelastic Monte Carlo sample as well as for the data, the E_{FCAL} spectrum extends to much higher values. Energy deposits in the forward calorimeter greater than 1 GeV were therefore ascribed to inelastic reactions in which part of the diffractively produced hadronic state X was detected in FCAL. The number of residual inelastic events in the data with FCAL energy smaller than 1 GeV was then estimated as

$$N_{in} = \left\{ \frac{N(E_{FCAL} < 1 \text{ GeV})}{N(E_{FCAL} > 1 \text{ GeV})} \right\}_{MC} \times \{N(E_{FCAL} > 1 \text{ GeV})\}_{DATA}.$$

The number of Monte Carlo and data events, $\{N(E_{FCAL} > 1 \text{ GeV})\}_{MC}$ and $\{N(E_{FCAL} > 1 \text{ GeV})\}_{DATA}$, were computed in the region $1 < E_{FCAL} < 8 \text{ GeV}$, where the inelastic Monte Carlo describes the data well. The overall contamination integrated up to $|t| = 0.5 \text{ GeV}^2$ was estimated to be $11\% \pm 1\%$ (stat.) $\pm 6\%$ (syst.). This was obtained using PYTHIA with $\beta = 2.5$. The systematic error reflects the sensitivity of the result to the value of the exponent β , which was varied between 2 and 3, and to the use of RHODI instead of PYTHIA. As a check, the sum of the elastic and inelastic Monte Carlo distributions of Fig. 5a and 5b were fitted to the data of Fig. 5c; the normalisations of the simulated distributions were free parameters of the fit. The χ^2 of the fit has a broad minimum around $\beta = 2.5$. This method gave a 12% contamination, consistent with the result given above. The result depends very little on the

shape of the generated t distribution: the estimate of the contamination varies by less than the quoted statistical error for a change of the exponential slope b between 4 and 6 GeV⁻².

The contamination was also studied as a function of t and W . It was found to vary from 6% for $|t| < 0.05$ GeV² to 19% for $|t| \simeq 0.5$ GeV²; it increases by $3 \pm 2\%$ as W increases from 65 to 75 GeV.

The contamination due to the elastic production of ϕ and ω mesons was estimated from Monte Carlo simulations. The selection cuts described in section 4 were applied to the simulated events after reconstruction. As an example, the contamination due to ω production was estimated as

$$\frac{A_\omega \sigma_\omega}{A_\omega \sigma_\omega + A_\rho \sigma_\rho},$$

where A_ω is the acceptance for elastic ω events. Assuming a cross section ratio of $\sigma_\omega/\sigma_\rho = 0.1$ [57], a contamination of $(1.3 \pm 0.2)\%$ is obtained. A similar procedure applied to ϕ events results in an estimated contamination of $(0.3 \pm 0.1)\%$, mainly due to the $\phi \rightarrow 3\pi$ decay mode. These contributions were not subtracted but were included in the systematic error. The contributions from inelastic ω and ϕ production were negligible.

Electron beam-gas and proton beam-gas contaminations were deduced from the pilot bunch event samples to which the cuts described in section 4 were applied. The number of events passing the cuts was then scaled by the ratio between the electron (proton) current in the paired bunches and the current in the electron (proton) pilot bunches. The contamination due to electron-gas interactions was estimated to be $2.3 \pm 0.5\%$, while that due to proton-gas events was found to be $0.3 \pm 0.2\%$.

All subsequent results are shown after subtraction of the contributions from inelastic proton diffraction and beam-gas interactions.

7 Results

7.1 Differential cross section $d\sigma/dM_{\pi\pi}$

Fig. 6 shows the acceptance corrected differential cross section $d\sigma/dM_{\pi\pi}$. The mass distribution is skewed compared to a Breit-Wigner distribution: there is an enhancement of the low mass side and a suppression of the high mass side. This distribution can be understood in terms of the interference between the resonant $\pi^+\pi^-$ production and a non-resonant Drell-type background [58] as discussed by Söding [59]. In order to extract the contribution of the resonant part of the differential cross section $d\sigma/dM_{\pi\pi}$, we followed a procedure similar to that described in refs. [6, 16, 25]. The function

$$d\sigma/dM_{\pi\pi} = f_\rho \cdot BW_\rho(M_{\pi\pi}) + f_I \cdot I(M_{\pi\pi}) + f_{PS} \quad (7)$$

was fitted to the measured mass distribution. The term

$$BW_\rho(M_{\pi\pi}) = \frac{M_{\pi\pi} M_\rho \Gamma_\rho(M_{\pi\pi})}{(M_{\pi\pi}^2 - M_\rho^2)^2 + M_\rho^2 \Gamma_\rho^2(M_{\pi\pi})} \quad (8)$$

is a relativistic Breit-Wigner function, with a momentum dependent width [60]

$$\Gamma_\rho(M_{\pi\pi}) = \Gamma_0 \left(\frac{p^*}{p_0^*} \right)^3 \frac{M_\rho}{M_{\pi\pi}}, \quad (9)$$

where Γ_0 is the width of the ρ^0 , p^* is the π momentum in the $\pi\pi$ rest frame and p_0^* is the value of p^* at the ρ^0 nominal mass M_ρ . The function

$$I(M_{\pi\pi}) = \frac{M_\rho^2 - M_{\pi\pi}^2}{(M_{\pi\pi}^2 - M_\rho^2)^2 + M_\rho^2 \Gamma_\rho^2(M_{\pi\pi})} \quad (10)$$

is a parametrisation of the interference term. The background term f_{PS} was taken to be constant. The free parameters in the fit were M_ρ , Γ_0 and the coefficients f_ρ , f_I and f_{PS} .

The results of the fit are presented in table 1 and in Fig. 6. The χ^2/ndf is 1.4, for $ndf=13$. The fitted values of the ρ^0 mass and width are in good agreement with the accepted ones [61]. The background term f_{PS} is consistent with zero, within a large error; similar results for f_{PS} were obtained by earlier experiments [6, 16] using the functional form (7).

The contribution of the resonant term increases with $|t|$, ranging from 86% of the events for $|t| = 0.01$ GeV² to 95% for $|t| = 0.5$ GeV².

The interference and the background terms were also studied as a function of W and of the decay pions' angular variables, $\cos\theta_h$ and ϕ_h , defined in section 7.4. No dependence on these variables was found.

The fit was repeated using different assumptions for the functional form of $d\sigma/dM_{\pi\pi}$.

- Parametrisation (7) is only an effective one, as it leaves the interference term independent of the resonant and non-resonant terms, which is strictly speaking inconsistent with the Söding mechanism. We therefore fitted the following functional form to the invariant mass distribution:

$$d\sigma/dM_{\pi\pi} = \left| A \frac{\sqrt{M_{\pi\pi} M_\rho \Gamma_\rho}}{M_{\pi\pi}^2 - M_\rho^2 + i M_\rho \Gamma_\rho} + B \right|^2, \quad (11)$$

where A , B , M_ρ and Γ_0 were free parameters of the fit. For Γ_ρ expression (9) was used. The non-resonant amplitude B was taken to be constant and real; it was also constrained to be non-negative. The results for the parameters are given in table 2. The χ^2/ndf was 1.4, with $ndf = 14$.

- The following alternative expressions for the width of the ρ^0 were adopted in the functions (8,10):

$$\Gamma_\rho(M_{\pi\pi}) = \Gamma_0 \left(\frac{p^*}{p_0^*} \right)^3, \quad (12)$$

$$\Gamma_\rho(M_{\pi\pi}) = \Gamma_0 \left(\frac{p^*}{p_0^*} \right)^3 \frac{2}{1 + (p^*/p_0^*)^2}. \quad (13)$$

- The Breit-Wigner was parametrised, following refs. [18, 60], as

$$BW_\rho(M_{\pi\pi}) = \frac{1}{p^*} \frac{M_{\pi\pi} M_\rho \Gamma_\rho(M_{\pi\pi})}{(M_{\pi\pi}^2 - M_\rho^2)^2 + M_\rho^2 \Gamma_\rho^2(M_{\pi\pi})} \quad (14)$$

and expression (13) was used for the width.

- The parametrisation given in ref. [24] was used:

$$d\sigma/dM_{\pi\pi} = f_\rho \cdot BW_\rho(M_{\pi\pi}) \cdot \left\{ 1 + C_1 \left[(M_\rho/M_{\pi\pi})^2 - 1 \right] + C_2 \left[(M_\rho/M_{\pi\pi})^2 - 1 \right]^2 \right\}. \quad (15)$$

The fit was repeated for the three mass dependent widths (9), (12) and (13).

- The phenomenological parametrisation proposed by Ross and Stodolsky [62] was used:

$$d\sigma/dM_{\pi\pi} = f_\rho \cdot BW_\rho(M_{\pi\pi}) \cdot (M_\rho/M_{\pi\pi})^n + f_{PS}, \quad (16)$$

where the factor $(M_\rho/M_{\pi\pi})^n$ accounts for the skewing of the shape of the ρ^0 signal. The term f_{PS} was taken to be constant. Here again the fit was repeated for the three mass dependent widths (9), (12) and (13). The parameter n was found to be $n = 4.9 \pm 0.5$, $n = 5.8 \pm 0.5$ and $n = 4.9 \pm 0.5$ for the three forms of the width, respectively.

In none of these cases did the quality of the fit change appreciably, as can be seen from table 3, in which the values of χ^2/ndf obtained for the various functional forms are summarised. The fitted values of the ρ^0 mass and width varied from 763 to 772 MeV and from 141 to 155 MeV, respectively. As we discuss in the next section, the values of the resonant part of the cross section were quite stable.

7.2 Integrated $\gamma p \rightarrow \rho^0 p$ cross section

The cross section $\sigma_{\gamma p \rightarrow \pi^+ \pi^- p}$ at $Q^2 = 0$, integrated over the $M_{\pi\pi}$ and t regions specified in (6) and averaged over the range $60 < W < 80$ GeV, can be obtained from the data as

$$\sigma_{\gamma p \rightarrow \pi^+ \pi^- p} = \frac{N_{\pi^+ \pi^-}}{L \epsilon \Phi},$$

where $N_{\pi^+ \pi^-}$ is the number of observed events after background subtraction, ϵ is the overall acceptance, L is the effective luminosity and $\Phi = 0.02419$ is the effective photon flux factor (see eq. 4) integrated over the specified W and Q^2 ranges. In order to extract the cross section for the *resonant* process $\gamma p \rightarrow \rho^0 p$, it was assumed that the ρ^0 meson decays to $\pi^+ \pi^-$ with a 100% branching ratio and the fit procedure described in section 7.1 (with expressions (7-10)) was used. The resonant part of the total $\pi^+ \pi^-$ signal is given by the parameter f_ρ multiplied by the integral of the relativistic Breit-Wigner curve, that is the area under the dotted curve in Fig. 6. There is some arbitrariness in the choice of the integration limits of the Breit-Wigner curve. The integral was carried out in the range $2M_\pi < M_{\pi\pi} < M_\rho + 5\Gamma_0$, where the ρ^0 mass and width values were taken from the fit; the quantity M_π is the pion mass. This requires an extrapolation beyond the measured region. The upper limit for the integration

range approximately corresponds to the mass of the nearest resonance, the $\rho(1450)$, with the same quantum numbers and quark content as the ρ^0 . The value of the cross section, for $2M_\pi < M_{\pi\pi} < M_\rho + 5\Gamma_0$, $|t| < 0.5 \text{ GeV}^2$ and averaged over the region $60 < W < 80 \text{ GeV}$, was measured to be:

$$\sigma_{\gamma p \rightarrow \rho^0 p} = 14.7 \pm 0.4 \text{ (stat.)} \pm 2.4 \text{ (syst.) } \mu\text{b}. \quad (17)$$

The systematic error is dominated by the uncertainties on the acceptance determination (13%), on the number of ρ^0 signal events (7%), and on the inelastic background determination (7%). If the integration is limited to the measured region, $0.55 < M_{\pi\pi} < 1 \text{ GeV}$, the cross section value is $12.4 \mu\text{b}$, i.e. lower by a factor $\xi = 1.19$. If the integral is computed up to $M_\rho + 4\Gamma_0$, the cross section decreases by 3%; if instead it is extended to $M_\rho + 6\Gamma_0$, the cross section increases by 2%.

The uncertainty on the acceptance determination has three main contributions:

1. the uncertainty on the calorimeter trigger efficiency near the threshold (9%);
2. the difference between the results obtained with DIPSI and with LEVEC (8%);
3. the sensitivity of the results to the cuts, notably that on the minimum number of CTD superlayers traversed by each track (6%).

The various alternative functional forms for $d\sigma/dM_{\pi\pi}$ described in the previous section were also used to extract the resonant part of the signal. The values obtained were centred around the result given in (17) but spanned the range $\sigma_{\gamma p \rightarrow \rho^0 p} = 13.6\text{-}15.4 \mu\text{b}$, corresponding to a $\pm 8\%$ maximum variation. The corresponding variation of ξ is $\pm 6\%$. The method of Spital and Yennie [63] was also used to obtain the cross section, yielding

$$\sigma_{\gamma p \rightarrow \rho^0 p} = \frac{\pi\Gamma_0}{2} \left. \frac{d\sigma}{dM_{\pi\pi}} \right|_{M_\rho} = 15.5 \pm 0.4 \mu\text{b}, \quad (18)$$

where the ρ^0 mass and width were those given in table 1. The result obtained with the Spital and Yennie method depends linearly on the value used for Γ_0 ; it is also sensitive to the value of M_ρ , since $d\sigma/dM_{\pi\pi}$ is a steep function of $M_{\pi\pi}$ in the region $M_{\pi\pi} \gtrsim 750 \text{ MeV}$, as can be seen from Fig. 6. If the values of M_ρ and Γ_0 given in ref. [61] are used, the cross section changes by less than 1%. If Γ_0 is kept fixed and M_ρ is varied between 760 and 780 MeV, the corresponding change in the cross section is 23%.

Table 3 summarises the results. We have taken the spread into account by including a $\pm 7\%$ contribution to the systematic uncertainty of the cross section.

The effect of real photon radiation by the incoming or the outgoing electron and that of vacuum polarisation loops is to lower the measured value of the cross section. The size of the correction was estimated to be smaller than 4% [64]. The correction was not applied; instead a 4% contribution was added to the systematic uncertainty.

Table 4 summarises the contributions to the systematic error. The total systematic error was obtained by summing all contributions in quadrature.

Result (17) for the cross section $\sigma_{\gamma p \rightarrow \rho^0 p}$ is presented in Fig. 7a together with a partial compilation of low energy measurements. The figure only includes results explicitly corrected for the interference term and the non-resonant background. We also show the ZEUS result [32], obtained indirectly using tagged photoproduction data from the 1992 data-taking period. Fig. 7b shows the result (18) obtained with the method of Spital and Yennie, along with a compilation of low energy results obtained with the same technique. The dashed curve in both figures is a parametrisation by Schuler and Sjöstrand [65]; the W dependence of the curve is based on Regge theory and on the assumption that the intercept of the pomeron is $\alpha(0) = 1 + 0.0808$ (the soft pomeron). The same general trend of the data is seen in the two figures. There are however differences in the results obtained by individual experiments; these differences at least in part reflect the ambiguity in the definition of the ρ^0 production cross section due to the finite width of the ρ^0 . The comparison between different experiments – and between the experimental results and the theoretical expectations – should thus be taken with caution. The curve satisfactorily reproduces the energy dependence of the data.

7.3 Differential cross section $d\sigma/dt$

Fig. 8a shows the acceptance corrected differential cross section $d\sigma/dt$, integrated over the ρ^0 mass region $2M_\pi < M_{\pi\pi} < M_\rho + 5\Gamma_0$. It was obtained by multiplying the differential cross section for the measured range $0.55 < M_{\pi\pi} < 1$ GeV by the factor $\xi = 1.19$ discussed in section 7.2. This assumes that, in each t bin, the ratio of the integral of the relativistic Breit-Wigner distribution over the range $2M_\pi < M_{\pi\pi} < M_\rho + 5\Gamma_0$ to that over the range $0.55 < M_{\pi\pi} < 1$ GeV is the same, i.e. that the mass and the width of the ρ^0 are the same in each bin. The contamination from inelastic ρ^0 production was subtracted bin by bin. Background and interference terms were also subtracted; their contribution was found by repeating the fitting procedure described in section 7.1 in each t bin, fixing the values of the ρ^0 mass and width to those given in table 1. Fig. 8b shows the results obtained for $d\sigma/dt$ by applying the Spital and Yennie method in each t bin.

The data were fitted with the function

$$\frac{d\sigma}{d|t|} = A_t \cdot e^{-b_t|t|} \quad (19)$$

in the range $|t| < 0.15$ GeV² and with the function

$$\frac{d\sigma}{d|t|} = A'_t \cdot e^{-b'_t|t| + c'_t t^2} \quad (20)$$

in the range $|t| < 0.5$ GeV². Both functions describe the data well. The results of the fits using expression (20) are shown in Fig. 8. Table 5 gives the values of the parameters obtained in the fits. The difference between the results of the fits to the points of Fig. 8a and b was taken as an estimate of the systematic uncertainty on the determination of the resonant fraction of the cross section in each bin. The other contributions to the systematic errors on A_t , A'_t and b_t ,

b'_t are the uncertainties on the acceptance and on the inelastic background determination. All contributions to the systematic errors were summed in quadrature. If the first bin is excluded from the fit to the points of Fig. 8a, the values of the slopes b_t and b'_t increase by 9% and 7%, respectively; the variation is smaller for the fit of Fig. 8b.

Fig. 9 shows the result for the slope b'_t as obtained from fitting eq. (20) to the points of Fig. 8a together with a compilation of fixed target results. All the results shown were obtained from fits of the form (20); the data were explicitly corrected for interference and non-resonant background, with the exception of those of ref. [5]. The data of refs. [5, 19] have the somewhat large minimum $|t|$ values of 0.2 and 0.15 GeV², respectively. For $W > 4$ GeV, the results do not depend strongly on W , as expected from Regge theory, which predicts a logarithmic dependence of the slope on W if one trajectory dominates.

7.4 Decay angular distributions

The ρ^0 decay angular distributions can be used to determine elements of the ρ^0 spin-density matrix [51].

In the s -channel helicity frame, in which the ρ^0 direction in the photon-proton centre-of-mass frame is taken as the quantisation axis, the decay angular distribution $H(\cos\theta_h, \phi_h, \Phi_h)$ is a function of the polar angle θ_h of the π^+ in the ρ^0 centre-of-mass frame, of the azimuthal angle ϕ_h between the decay plane and the γ - ρ^0 plane (the ρ^0 production plane) and of the angle Φ_h between the ρ^0 production plane and the electron scattering one. For $t = t_{\min}$, the photon and the ρ^0 are collinear and ϕ_h is not defined.

In the present experiment, the lepton scattering plane is not measured since neither the recoil proton nor the scattered electron are detected. Furthermore, the azimuthal angle ϕ_h can be determined only if the direction of the virtual photon is approximated by that of the incoming electron. It has been verified by Monte Carlo calculations that this is a good approximation. The experimental resolution in ϕ_h is approximately 40°; it is a function of t and improves with increasing $|t|$. The resolution in $\cos\theta_h$ is ≈ 0.03 . In the following we present the results for the one dimensional distributions $H_{\cos\theta_h}(\cos\theta_h)$ and $H_{\phi_h}(\phi_h)$, obtained from $H(\cos\theta_h, \phi_h, \Phi_h)$ after integrating over ϕ_h, Φ_h and over $\cos\theta_h, \Phi_h$, respectively. For unpolarised or transversely polarised electrons and a $J^P = 1^-$ state decaying into two pions, the functions $H_{\cos\theta_h}(\cos\theta_h)$ and $H_{\phi_h}(\phi_h)$ can be written as [51, 26]:

$$H_{\cos\theta_h} = \frac{3}{4}[1 - r_{00}^{04} + (3r_{00}^{04} - 1)\cos^2\theta_h], \quad (21)$$

$$H_{\phi_h} = \frac{1}{2\pi}(1 - 2r_{1-1}^{04}\cos 2\phi_h), \quad (22)$$

where r_{00}^{04} and r_{1-1}^{04} are ρ^0 density matrix elements. In particular r_{00}^{04} gives the probability that the ρ^0 is longitudinally polarised. Assuming s -channel helicity conservation (SCHC), r_{00}^{04} can be related to R , the ratio of the ρ^0 production cross sections for longitudinally and transversely polarised virtual photons [26]:

$$R = \frac{1}{\varepsilon} \frac{r_{00}^{04}}{1 - r_{00}^{04}}, \quad (23)$$

where ε is the virtual photon polarisation, i.e. the ratio of the longitudinally to transversely polarised photon fluxes. The present data have $\varepsilon = 0.998$, essentially constant over the W range covered by the measurement.

Fig. 10 shows the differential cross sections $d\sigma/d\cos\theta_h$ and $d\sigma/d\phi_h$. The curves are the results of the fits of the functions (21) and (22) to the data. A dominant $\sin^2\theta_h$ contribution is visible, indicating that the ρ^0 mesons are mostly transversely polarised. This is reflected by the result of the fit, which yields $r_{00}^{04} = 0.055 \pm 0.028$, where the error is statistical only. The fitted value of r_{1-1}^{04} is 0.008 ± 0.014 , consistent with zero, as expected on the basis of SCHC. If one uses expression (23) to determine R from the fitted value of r_{00}^{04} , one obtains $R = 0.06 \pm 0.03$. The average value of Q^2 for the data discussed in this paper, computed assuming the Q^2 dependence given in (4), is $\approx 0.1M_\rho^2 = 0.05 \text{ GeV}^2$. This gives, using expression (2), $R = 0.1$, consistent with our result.

7.5 Total $\rho^0 p$ cross section

By using the vector dominance model and the optical theorem, the measured value of $d\sigma/dt$ at $t = 0$ can be used to obtain the $\rho^0 p$ total cross section.

For $\rho^0 p$ scattering the optical theorem reads:

$$\left. \frac{d\sigma_{\rho^0 p \rightarrow \rho^0 p}}{dt} \right|_{t=0} = \frac{1 + \eta^2}{16\pi} \sigma_{tot}^2(\rho^0 p), \quad (24)$$

where η is the ratio of the real to the imaginary part of the forward $\rho^0 p$ scattering amplitude. We assume that $\eta = 0$. On the other hand, within VDM, elastic ρ^0 photoproduction is related to the elastic $\rho^0 p$ cross section; in particular, for $t = 0$:

$$\left. \frac{d\sigma_{\gamma p \rightarrow \rho^0 p}}{dt} \right|_{t=0} = \frac{4\pi\alpha}{f_\rho^2} \left. \frac{d\sigma_{\rho^0 p \rightarrow \rho^0 p}}{dt} \right|_{t=0}, \quad (25)$$

where $4\pi\alpha/f_\rho^2$ is the probability for the $\gamma \rightarrow \rho^0$ transition. We take $f_\rho^2/4\pi = 2.20$ (cf. e.g. [1], p. 393).

Using the intercept $d\sigma_{\gamma p \rightarrow \rho^0 p}/dt|_{t=0} = 133 \pm 11 \pm 27 \text{ } \mu\text{b}/\text{GeV}^2$ given in section 7.3, and combining equations (25) and (24), one finds $\sigma_{tot}(\rho^0 p) = 28.0 \pm 1.2$ (stat.) ± 2.8 (syst.) mb, where the errors reflect only the uncertainty on the measured value of the intercept. The systematic error does not include the uncertainties from the model dependence of the assumptions made nor from the values of η and $4\pi/f_\rho^2$.

The result is consistent with those found at lower energies (see e.g. [1, 66]). It is also in agreement with the expected value of 27.8 mb at $W = 70 \text{ GeV}$, obtained from the parametrisation [65] of $\sigma_{\rho^0 p}^{tot} \approx 1/2[\sigma^{tot}(\pi^+ p) + \sigma^{tot}(\pi^- p)] = 13.63(W^2)^{0.0808} + 31.79(W^2)^{-0.4525}$, based on the soft pomeron, the additive quark model [67] and on fits [68] to πp data at centre-of-mass energies ranging between 6 and 25 GeV.

8 Summary

The ZEUS detector at HERA has been used to study the photoproduction process $\gamma p \rightarrow \rho^0 p$. The integrated cross section as well as the differential cross sections $d\sigma/dM_{\pi\pi}$ and $d\sigma/dt$ at an average photon-proton centre-of-mass energy $\langle W \rangle = 70$ GeV have been measured.

The $\pi\pi$ mass spectrum is skewed, compared to a relativistic Breit-Wigner distribution, as also observed at low energy. The integrated $\gamma p \rightarrow \rho^0 p$ cross section, for $60 < W < 80$ GeV, $|t| < 0.5$ GeV² and $2M_\pi < M_{\pi\pi} < M_\rho + 5\Gamma_0$, is 14.7 ± 0.4 (stat.) ± 2.4 (syst.) μb . This result, in conjunction with the measurements at low energy, is consistent with the weak energy dependence expected on the basis of Regge theory and a pomeron intercept of 1.08 (the soft pomeron). This is at variance with the behaviour of the cross section for elastic photoproduction of J/ψ mesons [69] and elastic production of ρ^0 mesons for $Q^2 > 7$ GeV² [70].

The differential cross section $d\sigma/dt$ has an approximately exponential shape with a slope consistent with the results obtained by low energy experiments with $W > 4$ GeV. This is also in accord with Regge theory, which expects a logarithmic dependence of the slope on W .

The ρ^0 decay angular distributions have been studied. The ρ^0 mesons are mainly produced in a transversely polarised state; the probability to find the ρ^0 with longitudinal polarisation is $r_{00}^{04} = 0.055 \pm 0.028$. The value of r_{1-1}^{04} is 0.008 ± 0.014 , in accord with s -channel helicity conservation (SCHC). If SCHC is assumed, one obtains $R = 0.06 \pm 0.03$ for the ratio of the ρ^0 production cross sections for longitudinally and transversely polarised virtual photons, consistent with the value expected if VDM is assumed.

From the measured value of $d\sigma/dt$ at $t = 0$, within the VDM framework and by using the optical theorem, a value $\sigma_{\rho^0 p}^{tot} = 28.0 \pm 1.2$ (stat.) ± 2.8 (syst.) mb for the total $\rho^0 p$ cross section at $W = 70$ GeV is found, in agreement with extrapolations of the pion-proton total cross section data based on Regge theory and a soft pomeron.

Acknowledgements

We thank the DESY Directorate for their strong support and encouragement. The remarkable achievements of the HERA machine group were essential for the successful completion of this work, and are gratefully appreciated. It is a pleasure to thank N.N. Nikolaev, M.G. Ryskin and A. Sandacz for many enlightening discussions. We are also very grateful to K. Kurek for his calculation of the radiative corrections.

References

- [1] For a review, see e.g. T.H. Bauer et al., Rev. Mod. Phys. **50** (1978) 261.
- [2] H. Blechschmidt et al., Nuovo Cimento **52A** (1967) 1348.
- [3] L.J. Lanzerotti et al., Phys. Rev. **166** (1968) 1365.

- [4] ABBHHM Collab., R. Erbe et al., Phys. Rev. **175** (1968) 1669.
- [5] W.G. Jones et al., Phys. Rev. Lett. **21** (1968) 586.
- [6] F. Bulos et al., Phys. Rev. Lett. **22** (1969) 490.
- [7] G. McClellan et al., Phys. Rev. Lett. **22** (1969) 374.
- [8] SBT Collab., H.H. Bingham et al., Phys. Rev. Lett. **24** (1970) 955.
- [9] SBT Collab., J. Ballam et al., Phys. Rev. Lett. **24** (1970) 960.
- [10] DESY-MIT Collab., H. Alvensleben et al., Nucl. Phys. **B 18** (1970) 333.
- [11] R. Anderson et al., Phys. Rev. **D1** (1970) 27.
- [12] M. Davier et al., Phys. Rev. **D1** (1970) 790.
- [13] G. McClellan et al., Phys. Rev. **D4** (1971) 2683.
- [14] C. Berger et al., Phys. Lett. **39B** (1972) 659.
- [15] SWT Collab., Y. Eisenberg et al., Phys. Rev. **D5** (1972) 15.
- [16] J. Park et al., Nucl. Phys. **B 36** (1972) 404.
- [17] SBT Collab., J. Ballam et al., Phys. Rev. **D5** (1972) 545.
- [18] SBT Collab., J. Ballam et al., Phys. Rev. **D7** (1973) 3150.
- [19] G.E. Gladding et al., Phys. Rev. **D8** (1973) 3721.
- [20] G. Alexander et al., Nucl. Phys. **B 69** (1974) 445.
- [21] G. Alexander et al., Nucl. Phys. **B 104** (1976) 397.
- [22] W. Struczinski et al., Nucl. Phys. **B 108** (1976) 45.
- [23] B. Barish et al., Phys. Rev. **D9** (1974) 566.
- [24] R. M. Egloff et al., Phys. Rev. Lett. **43** (1979) 657.
- [25] OMEGA Collab., D. Aston et al., Nucl. Phys. **B 209** (1982) 56.
- [26] P. Joos et al., Nucl. Phys. **B 113** (1976) 53.
- [27] CHIO Collab., W. D. Shambroom et al., Phys. Rev. **D26** (1982) 1.
- [28] EMC Collab., J.J. Aubert et al., Phys. Lett. **161B** (1985) 203.
- [29] EMC Collab., J. Ashman et al., Z. Phys. **C 39** (1988) 169.
- [30] E665 Collab., G. Y. Fang et al., preprint FERMILAB-Conf. 93/305 (1993);
G. Y. Fang, in “Proceedings of the XIII International Conference on Particle and Nuclei”,
Perugia, Italy, 28th June-3rd July 1993, editor A. Pascolini, World Scientific, Singapore
(1994) p. 332.

- [31] NMC Collab., M. Arneodo et al., Nucl. Phys. **B 429** (1994) 503.
- [32] ZEUS Collab., M.Derrick et al., Z. Phys. **C 63** (1994) 391.
- [33] J.J Sakurai, Phys. Rev. Lett. **22** (1969) 981.
- [34] See e.g.
K. Goulianos, Phys. Rep. **101** (1983) 169.
- [35] A. Donnachie and P.V. Landshoff, Phys. Lett. **B 185** (1987) 403;
A. Donnachie and P.V. Landshoff, Nucl. Phys. **B 311** (1989) 509;
P.V. Landshoff, Nucl.Phys. B (Proc.Suppl.) **18C** (1990) 211;
P.V. Landshoff, in “Proc. of Joint LP Symposium and Europhysics Conference on HEP”,
Geneva 1991, editors S. Hegarty, K. Potter and E. Quercigh, World Scientific, Singapore,
1992, vol.2, p. 363.
- [36] J.R. Cudell, Nucl. Phys. **B 336** (1990) 1.
- [37] M.G. Ryskin, Z. Phys. **C 57** (1993) 89 and private communication.
- [38] B.Z. Kopeliovich et al., Phys. Lett. **B 324** (1994) 469.
- [39] S.J. Brodsky et al., Phys. Rev. **D50** (1994) 3134.
- [40] J. Nemchik, N.N. Nikolaev and B.G. Zakharov, Phys. Lett. **B 341** (1994) 228.
- [41] I.F. Ginzburg, D.Yu. Ivanov and V.G. Serbo, “Semihard quasi diffractive production of
neutral mesons by off shell photons”, to appear in Nucl. Phys. B.
- [42] The ZEUS Detector, Status Report, DESY (1993).
- [43] C. Alvisi et al., Nucl. Instrum. Methods **A 305** (1991) 30.
- [44] N. Harnew et al., Nucl. Instrum. Methods **A 279** (1989) 290;
C.B. Brooks et al., Nucl. Instrum. Methods **A 283** (1989) 477;
B. Foster et al., Nucl. Instrum. Methods **A 338** (1994) 254.
- [45] M. Derrick et al., Nucl. Instrum. Methods **A 309** (1991) 77;
A. Andresen et al., Nucl. Instrum. Methods **A 309** (1991) 101;
A. Bernstein et al., Nucl. Instrum. Methods **A 336** (1993) 23.
- [46] D. Kisielewska et al., “Fast Luminosity Monitoring at HERA”, DESY-HERA report 85-25
(1985),
J. Andruszków et al., DESY report DESY 92-066 (1992).
- [47] M. Costa, “Fotoproduzione di mesoni ρ in interazioni ep ad HERA”, Tesi di Dottorato,
University of Torino (1994), unpublished (in Italian).
- [48] M. Arneodo, L. Lamberti and M. G. Ryskin, to be submitted to Comp. Phys. Comm.
- [49] L. Lamberti, “Fotoproduzione esclusiva di mesoni vettori nell’esperimento ZEUS ad
HERA”, Tesi di Dottorato, University of Torino (1995), unpublished (in Italian).

- [50] G. Marchesini et al., *Comp. Phys. Comm.* **67** (1992) 465;
B.R. Webber, in “Proceedings of the Workshop ‘Physics at HERA”, DESY, 29-30 October 1991, editors W. Buchmüller and G. Ingelman, p. 1354;
L. Stanco, *ibidem*, p. 1363.
- [51] K. Schilling et al., *Nucl. Phys.* **B 15** (1970) 397;
K. Schilling and G. Wolf, *Nucl. Phys.* **B 61** (1973) 381.
- [52] ZEUS Collab., M.Derrick et al., DESY report DESY 95-084 (1995), submitted to *Z. Phys. C*.
- [53] T. Sjöstrand and M. Bengsston, *Comp. Phys. Comm.* **43** (1987) 367;
M. Bengsston and T. Sjöstrand, *Comp. Phys. Comm.* **46** (1987) 43;
T. Sjöstrand, in “Proceedings of the Workshop Physics at HERA”, DESY, 29-30 October 1991, editors W. Buchmüller and G. Ingelman, p. 1405.
- [54] T.J. Chapin et al., *Phys. Rev.* **D31** (1985) 17.
- [55] CDF Collab., F. Abe et al., *Phys. Rev.* **D50** (1994) 5535.
- [56] J. Forshaw and M. Ryskin, DESY report DESY 94-162 (1994), Rutherford Laboratory preprint RAL-94-058 (1994), and private communication.
- [57] “Total Cross-Sections for Reactions of High Energy Particles”, Landolt-Börnstein, New Series, Vol. 12b, editor H. Schopper (1987).
- [58] S.D. Drell, *Phys. Rev. Lett.* **5** (1960) 278.
- [59] P. Söding, *Phys. Lett.* **19** (1966) 702.
- [60] J.D. Jackson, *Nuovo Cimento* **34** (1964) 1644.
- [61] Review of Particle Properties, *Phys. Rev.* **D50** (1994) 1173.
- [62] R. Ross and V. Stodolsky, *Phys. Rev.* **149** (1966) 1172.
- [63] R. Spital and D.R. Yennie, *Phys. Rev.* **D9** (1974) 126.
- [64] K. Kurek, private communication.
- [65] G.A. Schuler and T.Sjöstrand, *Phys. Lett.* **B 300** (1993) 169;
G.A. Schuler and T.Sjöstrand, *Nucl. Phys.* **B 407** (1993) 539.
- [66] M. Arneodo et al., *Phys. Lett.* **B 332** (1994) 195.
- [67] E.M. Levin and L.L. Frankfurt, *JETP Letters* **2** (1965) 65;
H.J. Lipkin and F. Scheck, *Phys. Rev. Lett.* **16** (1966) 71;
J.J.J. Kokkedee, “The Quark Model”, W.A. Benjamin, New York (1969).
- [68] A. Donnachie and P.V. Landshoff, *Phys. Lett.* **B 296** (1992) 227.
- [69] ZEUS Collab., M.Derrick et al., *Phys. Lett.* **B 350** (1995) 120.
- [70] ZEUS Collab., M.Derrick et al., DESY report DESY 95-133 (1995), submitted to *Phys. Lett. B*.

Parameter	value	stat. error
M_ρ	0.764 GeV	0.003 GeV
Γ_0	0.142 GeV	0.007 GeV
f_ρ	9.86 μb	0.23 μb
f_I	3.47 $\mu\text{b GeV}$	0.34 $\mu\text{b GeV}$
f_{PS}	0.0 $\mu\text{b/GeV}$	5.5 $\mu\text{b/GeV}$

Table 1: Results of the fit to the mass spectrum for $60 < W < 80$ GeV and $|t| < 0.5$ GeV² (expressions (7-10)). Only statistical errors are given.

Parameter	value	stat. error
M_ρ	0.764 GeV	0.003 GeV
Γ_0	0.148 GeV	0.007 GeV
A	-3.10 $\mu\text{b}^{1/2}$	0.04 $\mu\text{b}^{1/2}$
B	2.0 $\mu\text{b}^{1/2} \text{ GeV}^{-1/2}$	0.2 $\mu\text{b}^{1/2} \text{ GeV}^{-1/2}$

Table 2: Results of the fit to the mass spectrum for $60 < W < 80$ GeV and $|t| < 0.5$ GeV² (expression (11)). Only statistical errors are given.

Functional form	χ^2/ndf (ndf)	$\sigma_{\gamma p \rightarrow \rho^0 p}$ [μb]	
		$0.55 < M_{\pi\pi} < 1 \text{ GeV}$	$2M_\pi < M_{\pi\pi} < M_\rho + 5\Gamma_0$
Expressions (7,8,9,10)	1.46 (13)	12.4 ± 0.3	14.7 ± 0.4
Expressions (7,8,12,10)	1.64 (13)	11.5 ± 0.2	14.5 ± 0.3
Expressions (7,8,13,10)	1.45 (13)	12.3 ± 0.6	14.3 ± 0.7
Expressions (7,14,12,10)	1.46 (13)	12.1 ± 0.6	13.6 ± 0.6
Expressions (11,9)	1.38 (14)	11.9 ± 0.3	14.3 ± 0.4
Expressions (15,9)	1.45 (13)	12.4 ± 0.5	14.7 ± 0.6
Expressions (15,12)	1.49 (13)	12.0 ± 0.5	15.4 ± 0.6
Expressions (15,13)	1.47 (13)	12.3 ± 0.5	14.4 ± 0.6
Expressions (16,9)	1.45 (13)	12.3 ± 0.6	14.6 ± 0.8
Expressions (16,12)	1.45 (13)	11.9 ± 0.6	15.2 ± 0.8
Expressions (16,13)	1.46 (13)	12.3 ± 0.6	14.3 ± 0.7
Expression (18)	-	-	15.5 ± 0.4

Table 3: Values of χ^2/ndf and results for the cross section $\gamma p \rightarrow \rho^0 p$ obtained by fitting the different functional forms described in the text to the data of fig. 6. The indicated errors are the statistical ones only.

Contribution from	Error
Luminosity	3%
Acceptance: trigger efficiency	9%
Acceptance: model dependence	8%
Acceptance: sensitivity to cuts	6%
Inelastic background subtraction	7%
Background due to elastic ω and ϕ production	1%
Procedure to extract the resonant part of the cross section	7%
Radiative corrections	4%
Total	17%

Table 4: Individual contributions to the systematic error on the integrated cross section.

Data from Fig. 8a			Data from Fig. 8b		
A_t	$= 139 \pm 6$ (stat.) ± 26 (syst.)	$\mu\text{b}/\text{GeV}^2$	A_t	$= 159 \pm 6$ (stat.) ± 28 (syst.)	$\mu\text{b}/\text{GeV}^2$
b_t	$= 10.4 \pm 0.6$ (stat.) ± 1.1 (syst.)	GeV^{-2}	b_t	$= 11.2 \pm 0.5$ (stat.) ± 1.1 (syst.)	GeV^{-2}
A'_t	$= 133 \pm 11$ (stat.) ± 27 (syst.)	$\mu\text{b}/\text{GeV}^2$	A'_t	$= 155 \pm 14$ (stat.) ± 29 (syst.)	$\mu\text{b}/\text{GeV}^2$
b'_t	$= 9.9 \pm 1.2$ (stat.) ± 1.4 (syst.)	GeV^{-2}	b'_t	$= 11.1 \pm 1.5$ (stat.) ± 1.4 (syst.)	GeV^{-2}
c'_t	$= 2.3 \pm 2.8$ (stat.)	GeV^{-4}	c'_t	$= 4.7 \pm 3.3$ (stat.)	GeV^{-4}

Table 5: The results of the fits to the data of Fig. 8a (left) and Fig. 8b (right) with function (20). For an explanation of the symbols see text.

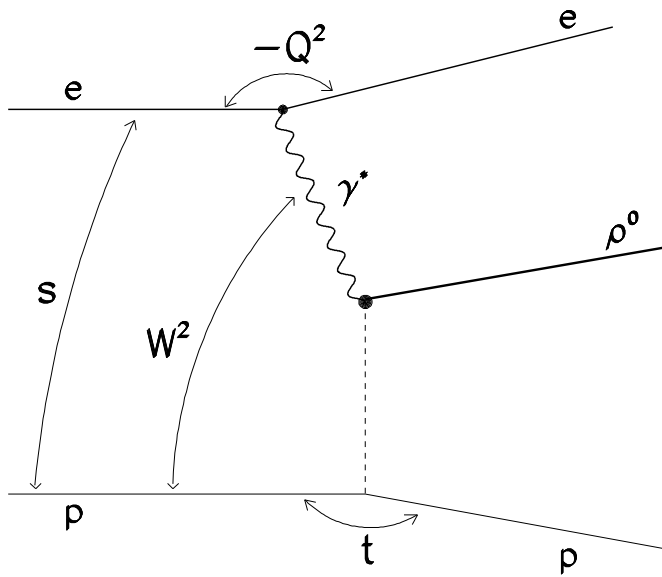


Figure 1: Elastic ρ^0 production in ep collision; the exchanged virtual photon is indicated as γ^* .

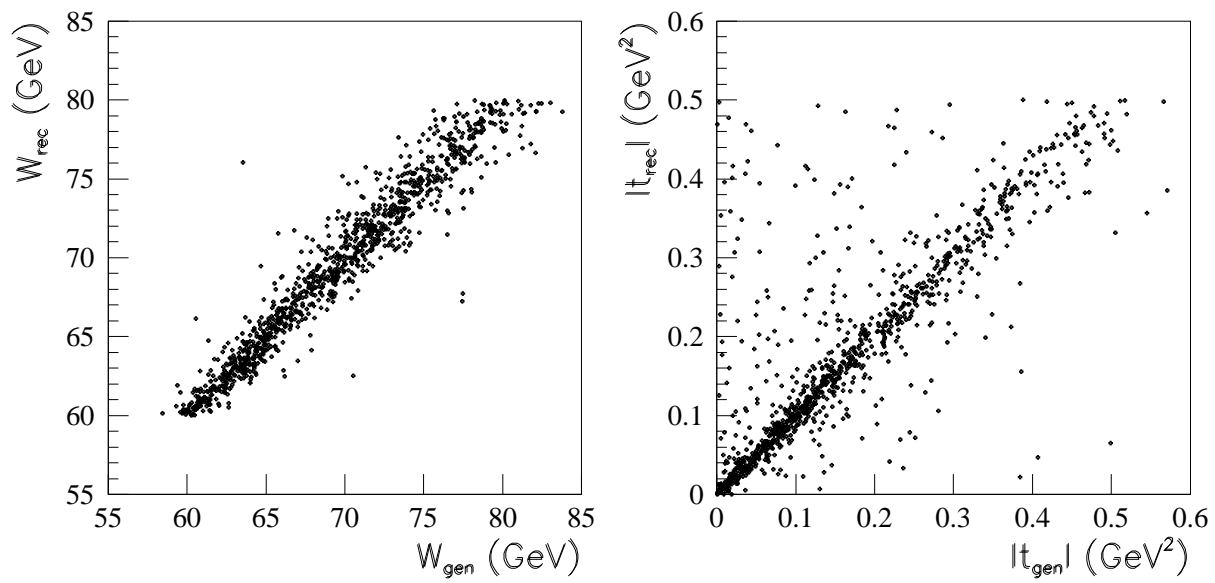


Figure 2: Scatter plot of reconstructed versus generated values of W and $|t|$ for Monte Carlo events.

ZEUS 1993

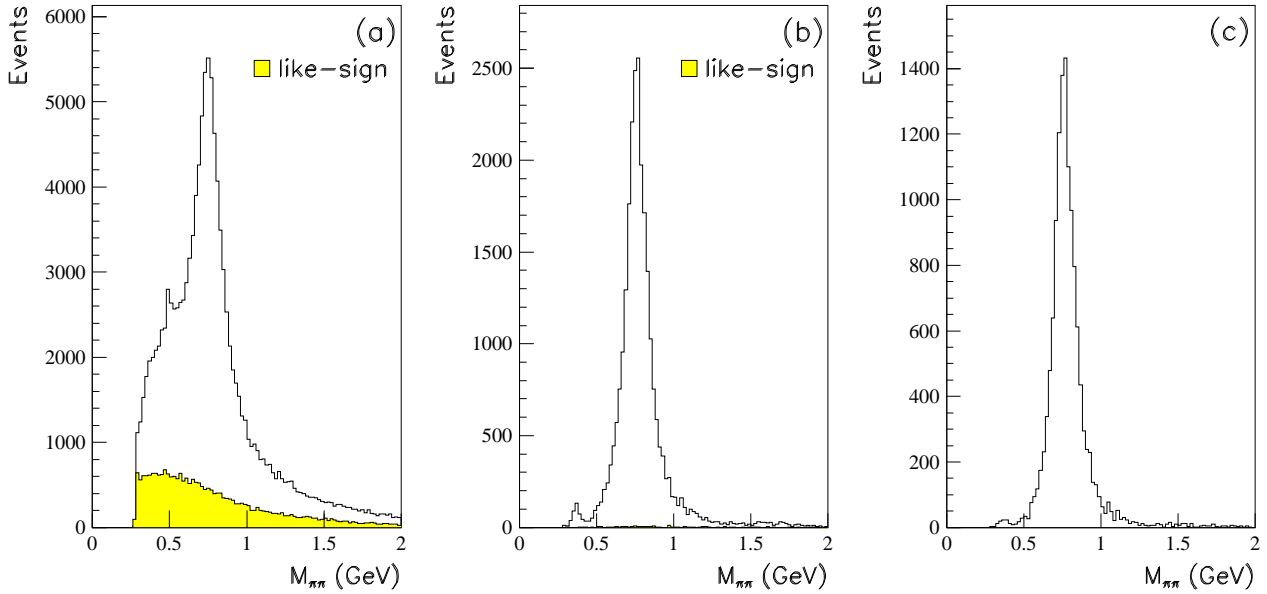


Figure 3: (a) The invariant $\pi^+\pi^-$ mass spectrum for all two track events selected by the untagged photoproduction trigger. (b) The distribution after applying all cuts, except those on W , $M_{\pi\pi}$ and p_T^2 . The shaded area in both plots (hardly visible in (b)) is the mass distribution of the like-sign pion pairs. (c) The distribution after all cuts, including those on W and p_T^2 (but not that on $M_{\pi\pi}$).

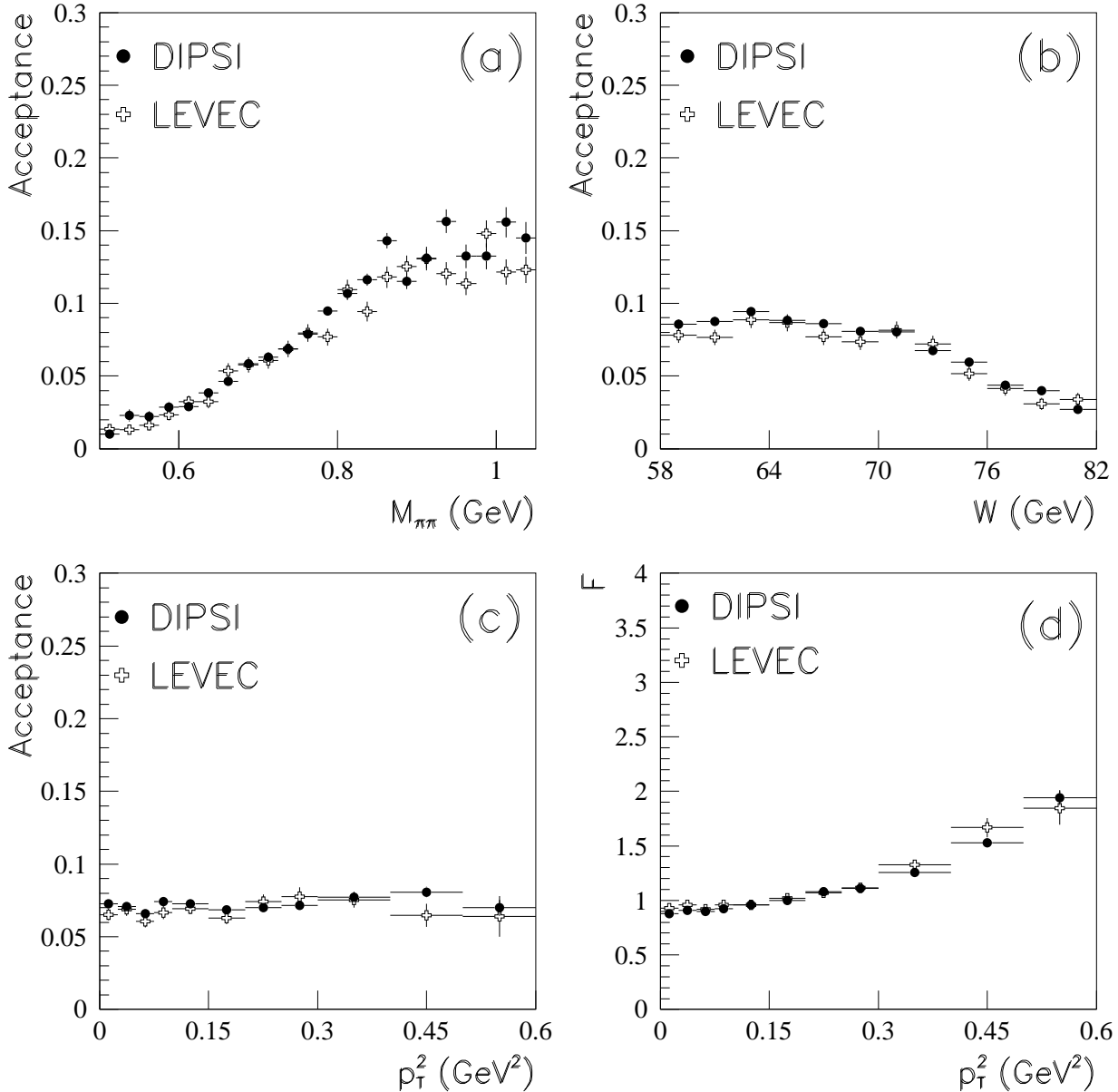


Figure 4: Acceptance as a function of $M_{\pi\pi}$ (a), W (b) and p_T^2 (c) obtained with the DIPSI and the LEVEC generators. The quantity F plotted in (d) is defined in the text. Only statistical errors are shown. The horizontal bars indicate the size of the bins.

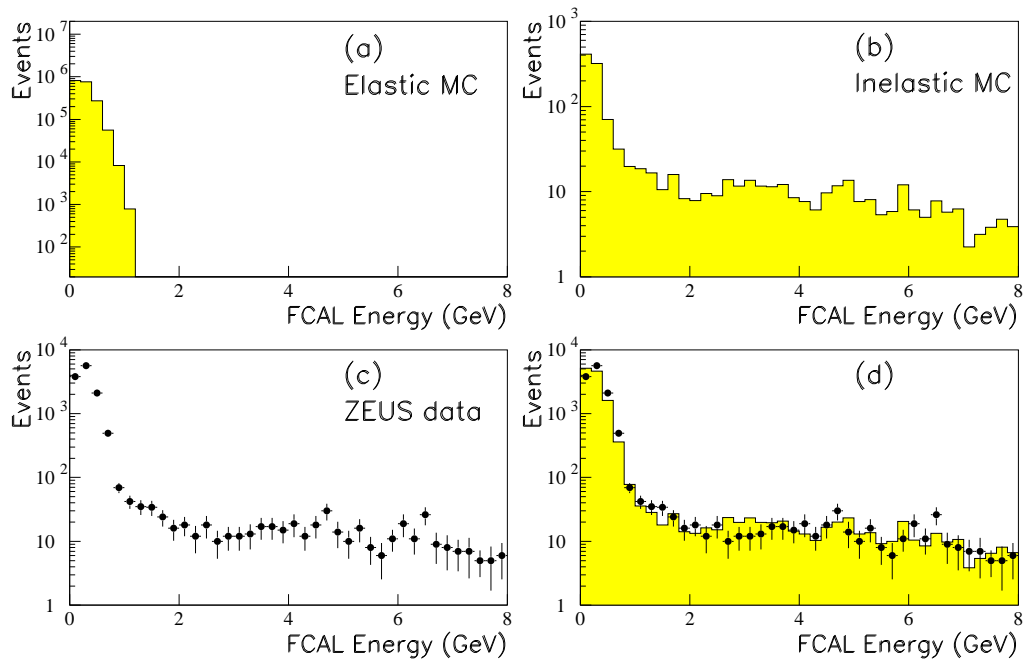


Figure 5: The energy spectrum in the forward calorimeter for: (a) elastic production ($ep \rightarrow e\rho^0 p$) simulated with DIPSI; (b) inelastic production ($ep \rightarrow e\rho^0 X$) simulated with PYTHIA; (c) data; (d) a mixture of 89% elastic and 11% inelastic Monte Carlo events (histogram) compared with data (dots).

ZEUS 1993

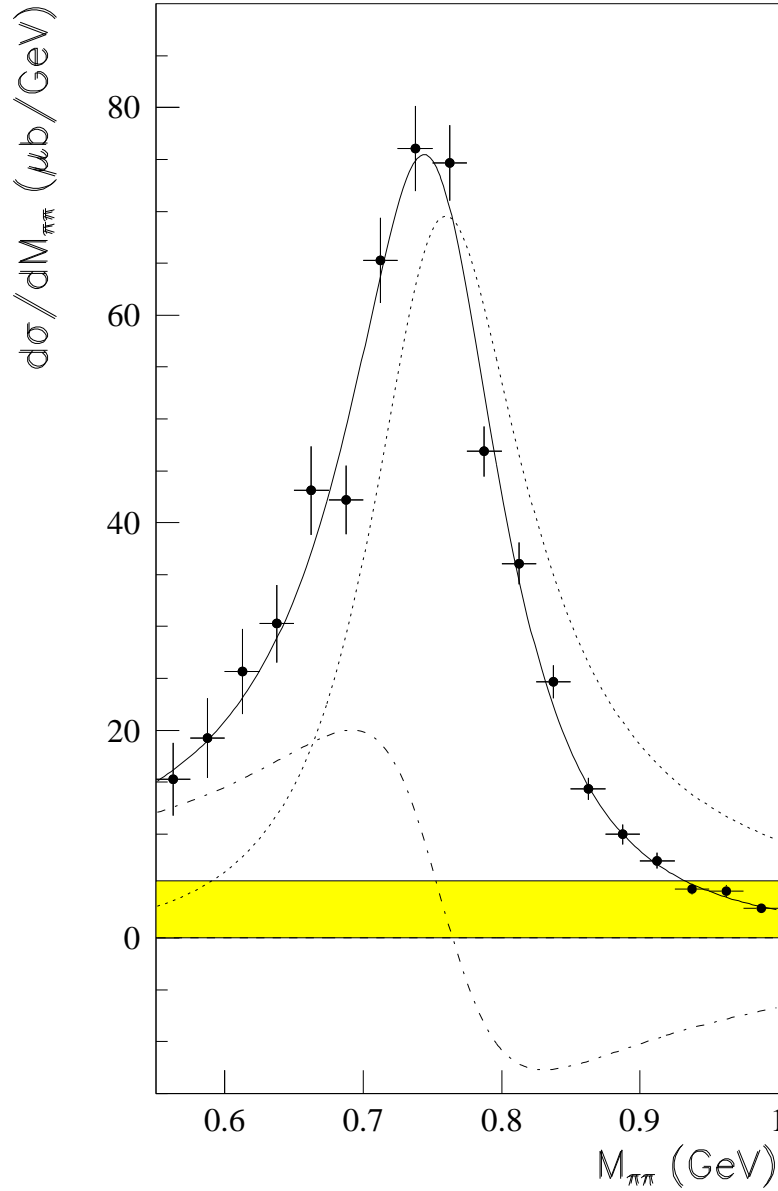


Figure 6: The acceptance corrected differential cross section $d\sigma/dM_{\pi\pi}$ for $60 < W < 80$ GeV and $|t| < 0.5$ GeV². The points represent the ZEUS data and the curves indicate the results of the fit to the data using expressions (7-10). The dotted line shows the contribution of the Breit-Wigner term and the dash-dotted line that of the interference term; the shaded band indicates the size of the statistical uncertainty on the background term f_{PS} . The solid curve is the sum of these three terms. Only statistical errors are shown. The horizontal bars indicate the size of the bins.

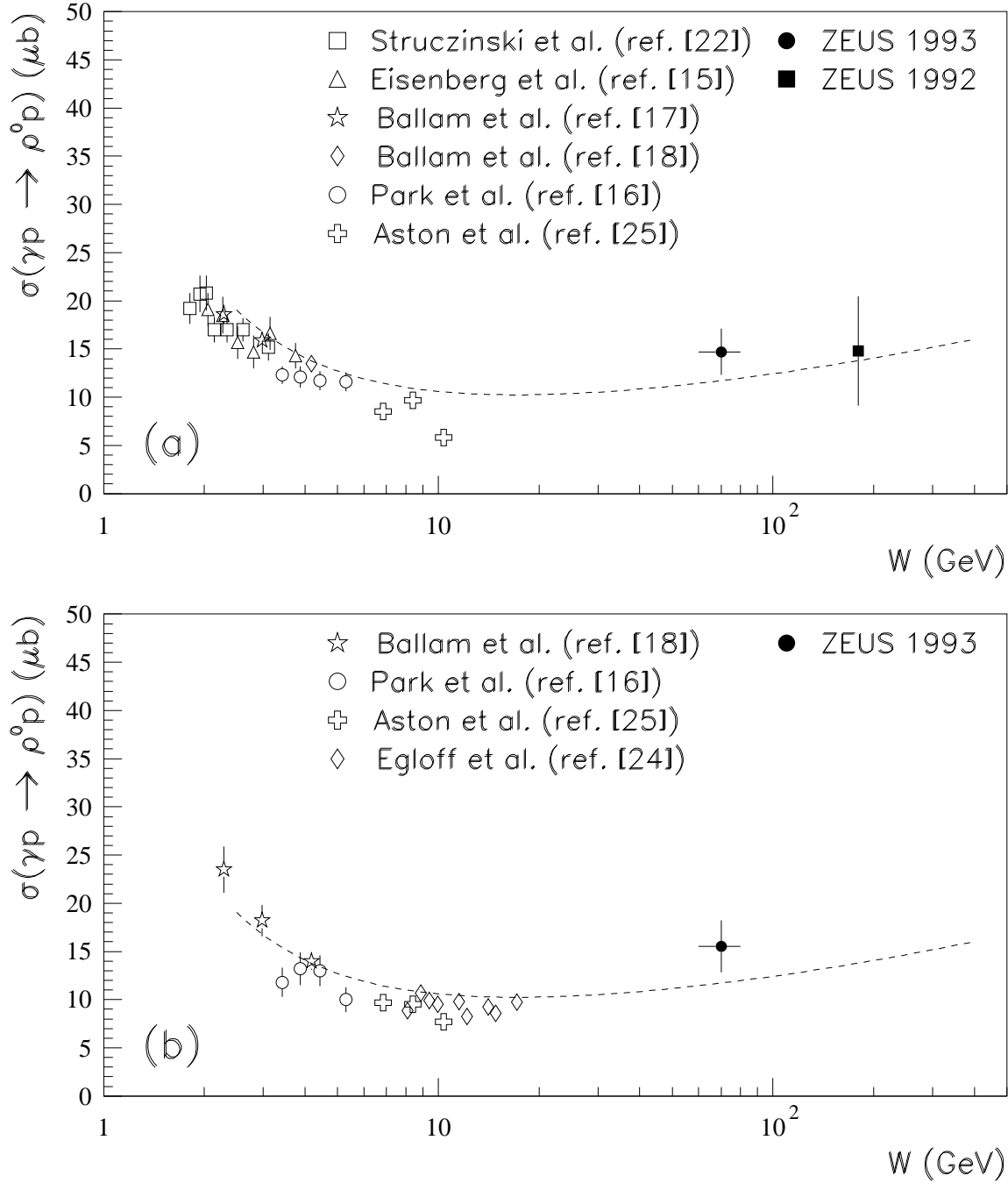


Figure 7: (a) The integrated cross section $\sigma_{\gamma p \rightarrow \rho^0 p}$ as a function of the centre-of-mass energy W . The ZEUS result (labelled “ZEUS 1993”) is that given in (17) for the range $2M_\pi < M_{\pi\pi} < M_\rho + 5\Gamma_0$, $|t| < 0.5 \text{ GeV}^2$. The ZEUS result [32] is also shown. The dashed line is the parametrisation from [65]. The vertical error bars of the ZEUS points indicate the quadratic sum of statistical and systematic errors. The horizontal bar indicates the size of the W region covered by the present measurement. (b) Same as (a) except that the results shown were obtained with the Spital and Yennie method.

ZEUS 1993

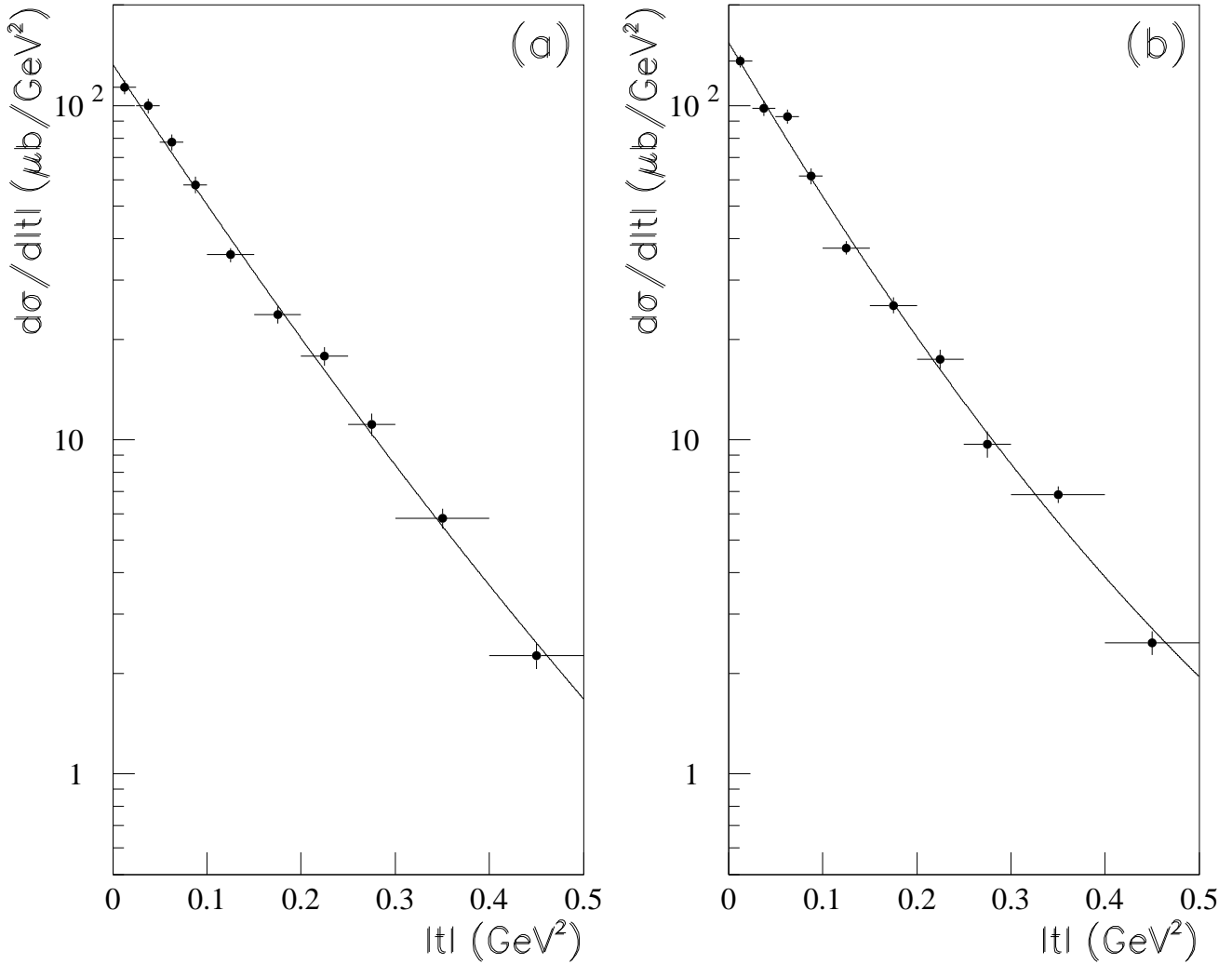


Figure 8: (a) The differential cross section $d\sigma/dt$ for $\gamma p \rightarrow \rho^0 p$ in the mass range $2M_\pi < M_{\pi\pi} < M_\rho + 5\Gamma_0$ and $60 < W < 80$ GeV. (b) The differential cross section $d\sigma/dt$ for $\gamma p \rightarrow \rho^0 p$ for $60 < W < 80$ GeV, as obtained by applying the Spital and Yennie method in each t bin. The continuous lines represent the results of the fit with the functional form (20). Only statistical errors are shown. The horizontal bars indicate the size of the bins.

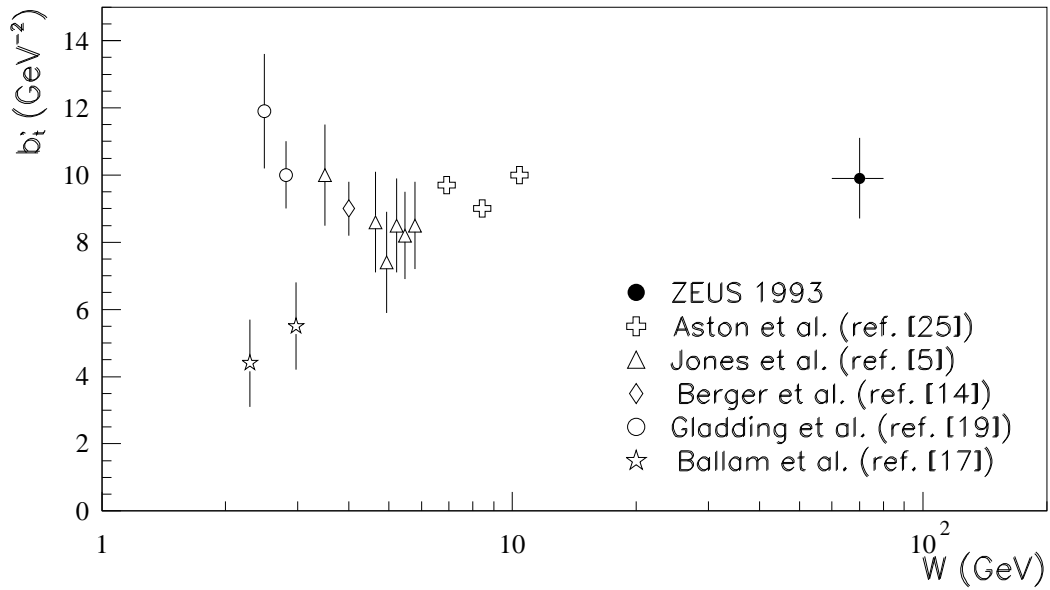


Figure 9: The slope b'_i as a function of W as obtained from fits with function (20). The ZEUS result is that found by fitting to the data of Fig. 8a. The vertical error bars indicate statistical errors only. The horizontal bar indicates the size of W region covered by the present measurement.

ZEUS 1993

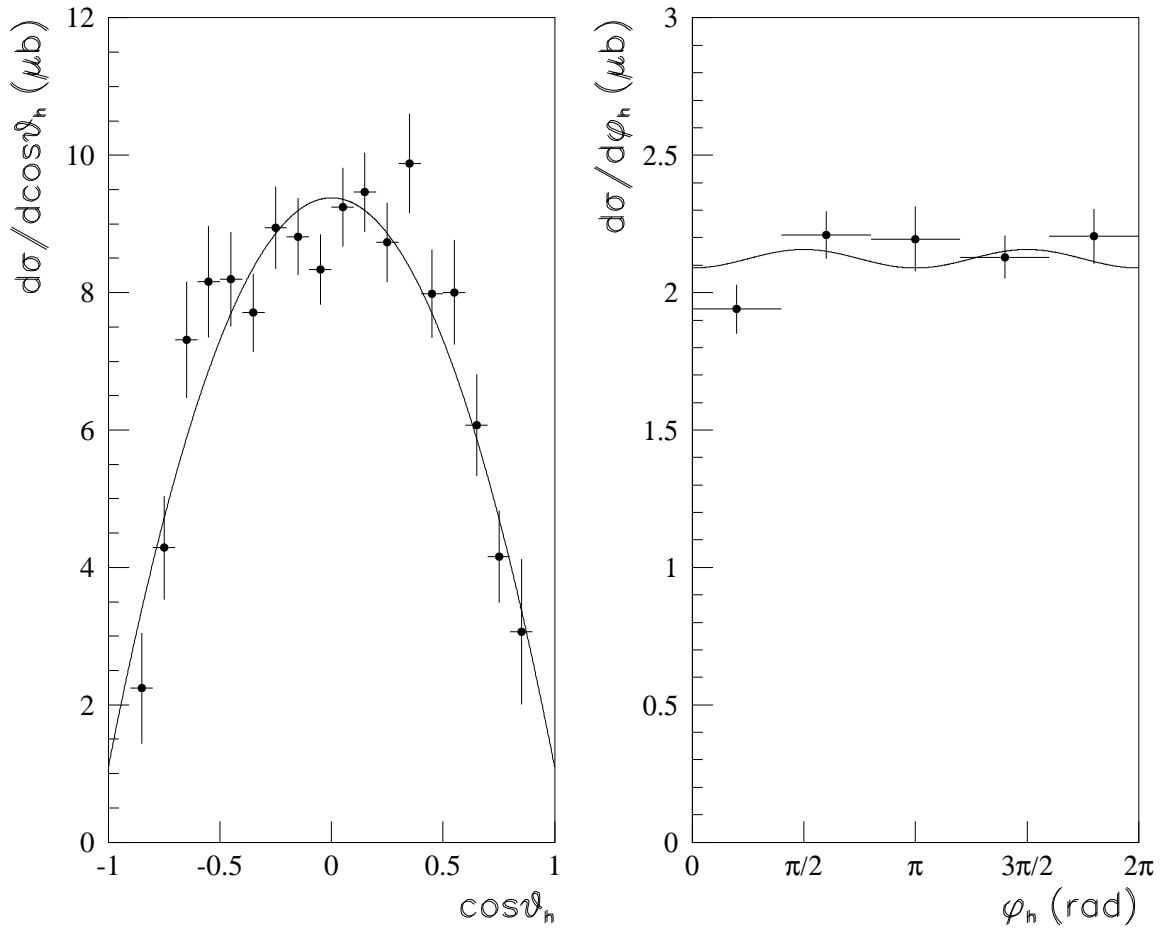


Figure 10: The differential cross sections $d\sigma/d\cos\theta_h$ and $d\sigma/d\phi_h$. The continuous lines represent the results of the fits discussed in the text. Only statistical errors are shown. The horizontal bars indicate the size of the bins.